Forschungszentrum Karlsruhe
in der Helmholtz-Gemeinschaft

Wissenschaftliche Berichte
FZKA 7295

Development of Modeling Tools to Describe the Corrosion Behavior of Uncoated EUROFER in Flowing Pb-17Li and their Validation by Performing of Corrosion Tests at T up to 550°C

W. Krauss, J. Konys, H. Steiner, J. Novotny, Z. Voss, O. Wedemeyer

Institut für Materialforschung

März 2007

Forschungszentrum Karlsruhe

in der Helmholtz-Gemeinschaft

Wissenschaftliche Berichte

FZKA 7295

Development of modeling tools to describe the corrosion behavior of uncoated EUROFER in flowing Pb-17Li and their validation by performing of corrosion tests at T up to 550°C

W. Krauss, J. Konys, H. Steiner, J. Novotny, Z. Voss, O. Wedemeyer

Institut für Materialforschung

Forschungszentrum Karlsruhe GmbH, Karlsruhe

2007

Forschungszentrum Karlsruhe GmbH
Postfach 3640, 76021 Karlsruhe

Mitglied der Hermann von Helmholtz-Gemeinschaft
Deutscher Forschungszentren (HGF)

ISSN 0947-8620

urn:nbn:de:0005-072958

Zusammenfassung

In einem zukünftigen Fusionsreaktor soll der ferritisch-martensitische Stahl Eurofer 97 als Strukturmaterial, das sich in direktem Kontakt mit dem flüssigen Brutmaterial Pb-17Li befindet, eingesetzt werden. Die Verwendbarkeit dieses niedrig aktivierbaren Stahles wird entscheidend von seiner Beständigkeit in dem strömenden Flüssigmetall Pb-17Li bestimmt werden. In verschiedenen zurückliegenden Untersuchungsreihen wurde das reine Korrosionsverhalten von ferritisch-martensitischen Stählen (z. B. Manet, Optifer, F82H-mod. oder Eurofer 97) bei Testtemperaturen von 480°C untersucht. Im Vordergrund standen dabei die Bestimmung auftretender Korrosionsmechanismen und die Auswertung der Korrosionsraten. Neue Designstudien zur TBM Auslegung weisen jedoch auf erhöhte Betriebstemperaturen von ca. 550°C mit variierenden Strömungsbedingungen hin. Eine Extrapolation der vorhandenen Ergebnisse in diese Bereiche ist jedoch nur mit großen Unsicherheitsfaktoren möglich und Daten zum Transport- und Ausscheidungsverhalten der Korrosionsprodukte, welche Korrosionsraten und sichere TBM-Betriebszustände mitbestimmen, sind nahezu nicht vorhanden. Die Analyse der verfügbaren Daten zeigte, dass eine Extrapolation aus vorhandenen 480°C-Daten auf höhere Temperaturen und/oder geänderte Strömungsbedingungen ohne Einsatz modellbasierter Auswertungskomponenten nicht oder nur mit großen Fehlern möglich ist.

Unter Berücksichtigung dieser Randbedingungen und dem Wunsch einer zukünftigen Übertragung des Korrosionsverhaltens auf TBM Bedingungen wurde eine Modellentwicklung zur Beschreibung des Korrosionsverhaltens von RAFM-Stählen in fließendem Pb-17Li begonnen. Die Modellkomponenten basieren dabei auf physikalisch-chemischen Materialparametern und berücksichtigen auch den Transport und das Ausscheidungsverhalten inklusive der unterschiedlichen Temperaturniveaus in dynamischen Systemen. Die modular strukturierten Komponenten wurden im Korrosionscode MATLIM zusammengeführt. In der ersten Ausbaustufe bildet dieser Code die Verhältnisse des verwendeten Testloops PICOLO ab. Zu seiner Validierung wurden sowohl die bereits vorhandenen Korrosionsraten (480°C Tests) als auch neu bei 550°C gemessene Korrosionswerte hinzu gezogen. Die ausgeführten Korrosionsversuche von Eurofer 97 bei 550°C in strömenden Pb-17Li bei einer Flussrate von 0.22 m/s zeigten dramatisch erhöhte Korrosionsraten von ca. 500 µm/Jahr im Vergleich zu etwa 90 µm/Jahr bei 480°C. Des Weiteren kam es während des Versuchsbetriebs zu Strömungsblockierungen im Kreislauf durch Ausscheidungsprodukte in kälteren Zonen. Beide Ergebnisse zeigen damit anschaulich das vorhandene Risiko beim Betrieb von TBMs unter diesen Betriebsbedingungen und fordern evtl. Korrosionsschutzschichten zur Begrenzung der Korrosion. MATLIM war in der Lage, mit ca. 80 µm/Jahr (480°C) bzw. 520 µm/Jahr (550°C) die experimentell ermittelten Werte sehr gut voraus zu berechnen. Weiterhin konnte MATLIM auch das beobachtete Ausscheidungsverhalten im kalten Bereich recht gut voraussagen. Speziell im Bereich Transport- und Ausscheidungsverhalten weisen die neuen Ergebnisse auf deutliche Wissenslücken beim Betrieb von dynamischen Systemen hin und fordern weitere Untersuchungen zum Ausscheidungsverhalten.

Abstract

Reduced activation ferritic-martensitic steels (e.g. EUROFER) are considered for application in future fusion technology as structural material, which is in contact with the breeding material Pb-17Li. Various corrosion experiments have been made in the past, however, evaluation of these tests, which were mostly conducted up to moderate temperatures of up to 480°C, was performed with respect to determine corrosion rates and mechanisms e.g. dissolution of some elements out of the steels and comparison of the results with earlier tested RAFM-steels of type F82H-mod. OPTIFER, and MANET. In the mean time the envisaged operation limits e.g. in temperature increased to roughly 550°C and flow regimes may change. Thus extrapolations of the RAFM-steel corrosion behavior determined in the past to the new working conditions may be problematic due to large uncertainties or reliability and, additionally, only low knowledge on transport of dissolved components in the Pb-17Li flow is present. In contrast to earlier investigations, these changes in requirements need the going over from (only) mechanism based corrosion tests to model supported tests. Furthermore, the whole loop has to be considered in the evaluation of the corrosion tests together with other occurring phenomena and mechanisms as transport effects and precipitations.

Therefore, under this task the development of modeling tools for describing Pb-17Li corrosion (dissolution, material transport and precipitations) was started. The modular structured tools are based on physical, chemical and thermo-hydraulic parameters and, in the first stage, the development was focused on the dissolution of EUROFER and validation with older test results obtained at 480°C in our PICOLO loop earlier. In the second stage the new 550°C test results – obtained in the part corrosion testing of this task - were used for validation at a second temperature level and transport phenomena were considered.

This report consists of the two subtasks a) corrosion testing and b) modeling with the main achievements given for each part in the next paragraphs.

A) Corrosion testing at 550°C

The corrosion testing of bare cylindrical EUROFER samples was performed in the upgraded PICOLO loop for testing at the new blanket relevant temperature of 550°C in flowing Pb-17Li with a flow rate of about 0.22 m/s – the same flow value and configuration as used in earlier 480°C tests. The post exposure analyses of the samples from the 550°C champagne showed that the corrosion mechanisms are the same as detected at the lower exposure temperature of 480°C namely homogeneous corrosion attack and dissolution of steel components. In the test series durations up to 5,000 h were examined and a corrosion rate was evaluated of about 500 µm/a. This value is more than 5 times the rate observed in 480°C tests and represents a dramatically increase in corrosion rate by a slight increase of only 70 K in testing temperature. Under these conditions 1 m² TBM surface would generate about. 4 kg Fe dissolved in Pb-17Li per year. The operation of PICOLO loop showed clearly the dangerous situation of loop blockages by precipitations formed in the cooler sections after short times (approx. 3,000 h) due to the high amount of dissolved and transported corrosion products. Looking in more detail the first test results obtained at 550°C with a short time base of 5,000 h will not have yet the high reliability for

extrapolation up to several 10,000 h known from the 480°C tests as required for TBM design. However a new test series was launched to increase reliability and also statistics with exposure times up to 10,000 h. A global valuation of the evaluated corrosion rates at 550°C in comparison with 480°C values and data coming from other laboratories using the empirical Sannier correlation showed that the new 550°C data are well positioned in the complex temperature and flow rate depending corrosion attack picture. These corrosion figures illustrate that corrosion of bare RAFM steels at high temperatures – also at reduced flow rates in real TBM's - may be a serious and challenging task in handling of blanket systems beside tritium permeation and may require corrosion protection measures by coatings.

B) Development of modeling tools and their validation

The developed modeling tools are based on physical and electrochemical parameters to describe the occurring mechanisms and phenomena in a non-isothermally operated loop. The developed and validated tools will simulate in the basic model configuration dissolution (corrosion attack), transportation of corrosion products and precipitation effects in dependence of the thermo hydraulic parameters (e.g. flow velocity, temperature profile) of the test loop PICOLO. The validation process showed that the selection of 'good' physical properties e.g. diffusion coefficients will have a critical impact on the results modeled. The validation of the two different test temperatures indicated that probably values evaluated by Feuerstein will be most reliable ones. Under these boundary conditions the developed tools reproduced the measured corrosion rates (90 µm/a at 480°C and 500 µm/a at 550°C) rather well with about 80 µm/a and 520 µm/a, respectively. The parameterization of the whole loop showed the sections where dissolution or precipitation takes place in dependence of the local temperatures. The modeling of precipitation needs more experimental input to decide whether needle like particles are formed or if precipitates grow on the surfaces. Additionally, validation with varied flow rates should be performed in future to have a tool for reliable prediction of effects in TBM's working far away of tested loop configuration.

Contents

A Corrosion testing

1. Introduction

In a future fusion system reduced activation ferritic-martensitic or ferritic (RAFM) steels are considered as structural materials. The alloy EUROFER 97, a 9 Cr W V Ta alloy, which was developed on base of the experience with RAFM alloys of e.g. Optifer type, is at the moment the favored FM-steel. During the last years the thermal and mechanical behavior of EUROFER 97 was examined [1] and first corrosion testing in the Pb-17Li loop PICOLO [2, 3] at moderate temperature (480°C) was performed. However, the corrosion tests were only evaluated regarding corrosion rates and occurring mechanisms e.g. dissolution of alloy components neglecting the impact of the whole loop. Additionally, envisaged new operation conditions have to be considered in the corrosion analyses e.g. service temperature in a fusion reactor were increased to about 550°C. Reliable extrapolations to the new operation regimes and considering the loop behavior (e.g. temperature profiles, flow rates) need model support and some specific corrosion tests for validating the model. .

The part 'Experimental' is dedicated to the PICOLO upgrade for working at 550°C and to the performed corrosion tests with exposure times of up to 5,000 h inclusively re-evaluation of earlier test campaigns (extraction of modeling relevant additional data) and later to post mortem analyses of the exposed and removed samples.

2. Experimental

2.1 PICOLO upgrade to 550°C:

In the past corrosion tests were performed in PICOLO loop at 480°C and the loop was not designed for working above a layout temperature of about 500°C for longer times. Thus a loop redesign and upgrade to the newly envisaged testing conditions had to be performed. However, the general loop configuration was kept constant. A sketch drawing of the loop is given in Fig. 1 with indexing the main components together with the front view onto the loop. The components in the low temperature section (about T < 400°C) are fabricated from 18 / 12 Cr Ni steel. The temperature in the cold leg (about 350°C) is determined by the layout temperature limit of the electro-magnetic pump (EMP). The working range of the EM-pump lies between 0.01 and 1.0 m/s. Standard test conditions were about 0.22 m/s in the past for examination of corrosion behavior of RAFM steels. The parts in the high temperature section (Electrical heater, counter flow heat exchanger and test section) are made from a Si-containing 10 % Cr-steel (1.4713). The test section (TS) is vertically orientated with a flow from top to bottom, the inside tube diameter is 16 mm, the length is about 420 mm. The stack of the test samples is centered in the test section. Mounting of the samples is done trough the expansion vessel, which is located in a glove box under controlled and purified argon gas atmosphere. A constant temperature profile ($\Delta T < 1$ K) is present in the test section. Dissolved and in the cold leg precipitated Fe-particles will be collected in the magnetic trap device. This device was originally installed to collect Fe particles and thus to reduce the risk of loop closures (especially valid for the counter flow heat exchanger) by precipitations.

Tab. 1 shows the main parameters of PICOLO loop with a total length of 12.2 m. The temperature profile of the loop measured by thermocouples is given in Fig. 2 for testing condition 480°C.

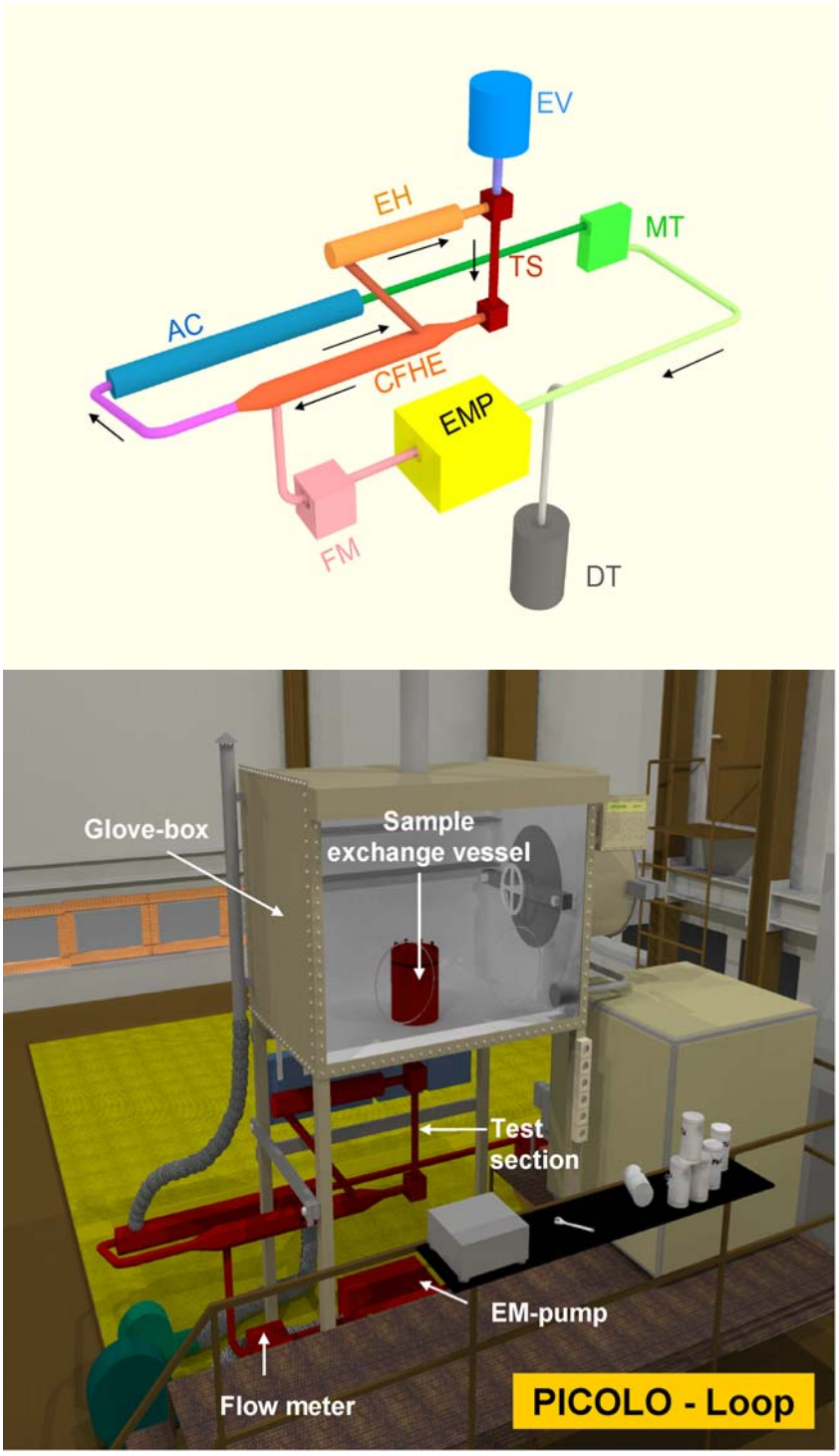

Fig. 1: Schematically layout and view of PICOLO loop
DT = Dump Tank, EMP = Electro-Magnetic Pump,
FM = Flow Meter, CFHE = Counter Flow Heat Exchanger,
AC = Air Cooler, EH = Electrical Heater,
EV = Expansion Vessel, TS = Test Section, MT = Magnetic Trap

Tab. 1: Main parameters of PICOLO loop	
Test temperature	**480 - 550°C**
Loop temperatures at operation of 550°C	
T_{max} in test section	**550°C**
T_{low} at EM-pump	**350°C**
Pb-17Li volume	**20 litres**
Length of loop	**12.2 m**
Flow velocity range (design value)	**0.01 to 1 m/s**
Test velocity	**0.22 m/s**
Loop materials	
Cold legs	**18 12 CrNi steel**
Hot legs	**10 % Cr steel**
Total loop operation	
at 480°C	**> 120,000 h**
at 550°C new test temp	**> 5,000 h**

Due to the new test specifications (test temperature 550°C) in the actual task a re-layout of the loop had to be performed. Most affected components were the electric heating and control system (required additional power was about 50 %), upgrade of the air cooling device for permanent working (guarantee of not more than 350°C in electromagnetic pump), changing several tube sections to Cr-steels (elimination of fast attacked CrNi steels), and inserting a new test section. Fig. 3 gives the temperature distribution for the 550°C testing scenario after loop upgrading. The inlet temperature into the test section was slightly above 550°C for the whole test series specified with 550°C. Similar to the 480°C tests a constant temperature profile over the 420 mm length of the test section was present with $\Delta T = 1$ K.

After finishing the technological work inclusive some commissioning and conditioning tests PICOLO loop was loaded with samples for corrosion testing at 550°C. Up to yet samples were removed with exposure times up to 5,000 h in intervals of about 500 or 1,000 h. In contrast to the 480°C the required pumping power increased more significantly and faster than assumed to keep constant the Pb-17Li flow rate of120 l/h or to guarantee the flow velocity of 0.22 m/s in the test section. It is known from earlier test series that the pumping power is correlated to the dissolved and precipitated corrosion products mainly deposited in the magnetic trap. After about 2,500 h testing time – due to pumping power limits – a switch off was necessary. The magnetic trap was dismounted and replaced by a fresh component. Up to 5,000 h no new loop blockage appeared by precipitations, however, pumping power had to be increased continuously.

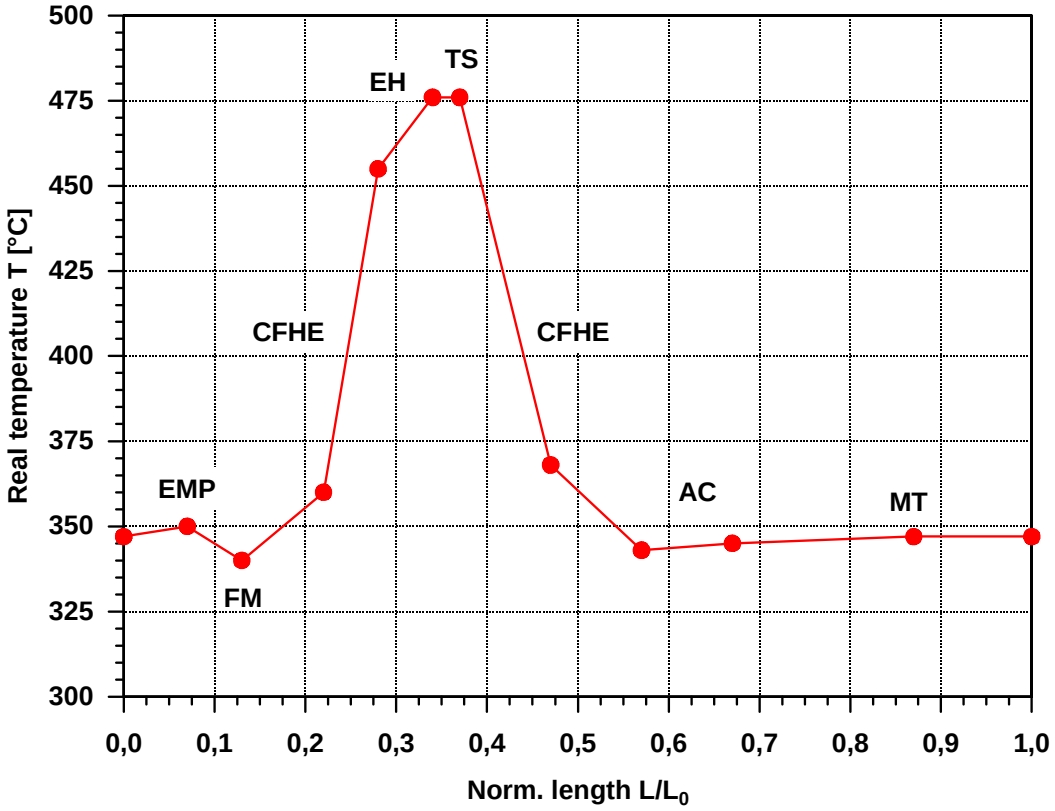

Fig. 2: Temperature profile of PICOLO loop with 480°C temperature in test section. Apprehensions see text to Fig. 1.

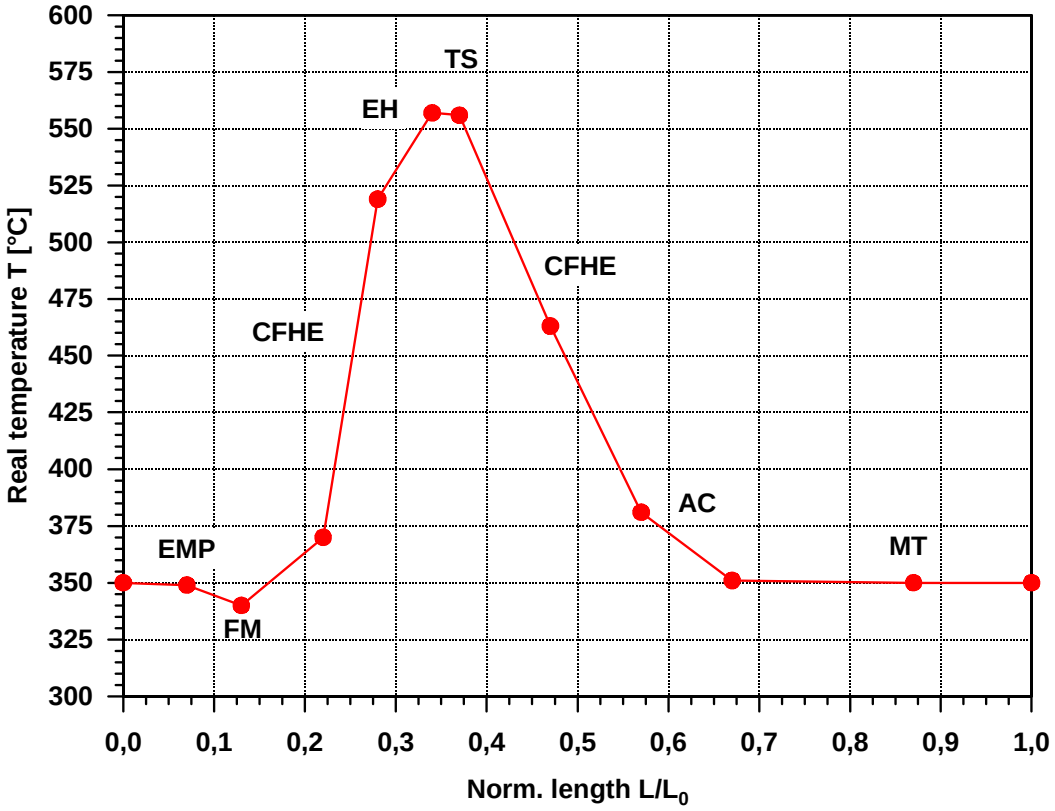

Fig. 3: Temperature profile of PICOLO loop with 550°C temperature in test section. Apprehensions see text to Fig. 1.

2.2 Sample preparation

2.2.1 Raw material

The older (480°C) and the actual (550°C) test samples were fabricated from plate material (thickness 14 mm, charge nr. E 83698, plate nr. 14, lot no. 249) produced by Böhler Edelstahl GmbH, Austria. The austenitization conditions were 980°C, 27 min and cooling in air. Tempering was done at 760°C for 90 min with subsequent air cooling. No additional thermal heat treatment was performed. Tab. 2 gives the chemical composition of the used raw material EUROFER 97 inclusive comparison to RAFM-alloys tested earlier. The test samples were fabricated by turning and subsequently cleaned in an ultrasonic bath (acetone) and dried. The test samples were screwed together to a stack of 12 pieces for loading into PICOLO loop. The total length of the test rod is about 400 mm. The diameter of the samples is 8.0 mm.

Tab. 2: Analyses of FM steels used in PICOLO loop corrosion tests

Steel	Cr	Mn	V	W	Ta	Mo	C	Ni
MANET I	10.6	0.82	0.22	--	--	0.77	0.13	0.87
Optifer IVa	8.5	0.57	0.23	1.16	0.16	--	0.11	--
F82H-mod.	7.7	0.16	0.16	1.95	0.02	--	0.09	--
EUROFER 97	8.82	0.47	0.20	1.09	0.13	--	0.11	0.02

In contrast to the earlier 480°C testing removal and replacement of samples in the stack is performed in intervals of about 500 h considering the expected stronger corrosion attack. The removed samples were carefully cleaned from excess Pb-17Li in the glove box with respect not to destroy adherent scales. Fig. 4 shows samples before and after exposure to Pb-17Li.

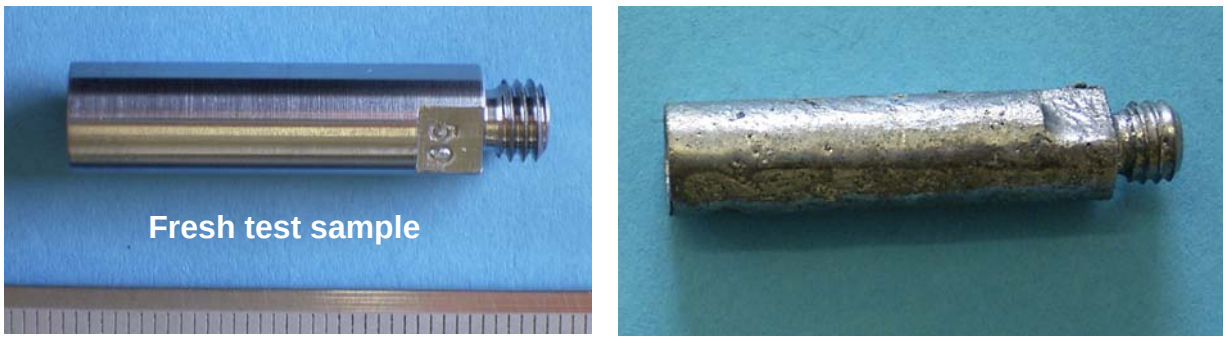

Fig. 4: EUROFER 97 samples
Left: before loading
Right: removed sample after 1,025 h, 550°C

2.2.2 Surface analyses

The samples used in PICOLO tests were fabricated by turning and grinding from plate material as specified above. Before inserting of the samples into the loop a cleaning in acetone with subsequent drying in an air flow was performed. In the test scenarios and also in modeling oxide free surfaces are assumed. Surface analyses of EUROFER samples were performed by AES to determine surface scales and thickness and composition. Fig. 5 shows the SEM pictures of the analyzed surface by different magnification. The pictures confirm the earlier performed measurements on surface roughness which showed average values of R_a = 0.5 µm and maximal peak values of R_z = 2.4 µm [2].

The AES examination indicates that a very thin contaminated surface scale is present. One kind of contamination is of absorbed CH_x molecules. The other component is oxygen. The thickness of this oxide scale is in the range of up to about 5 nm. It is a Fe-oxide with a small amount of Cr. The concentration profiles are also given in Fig. 5.

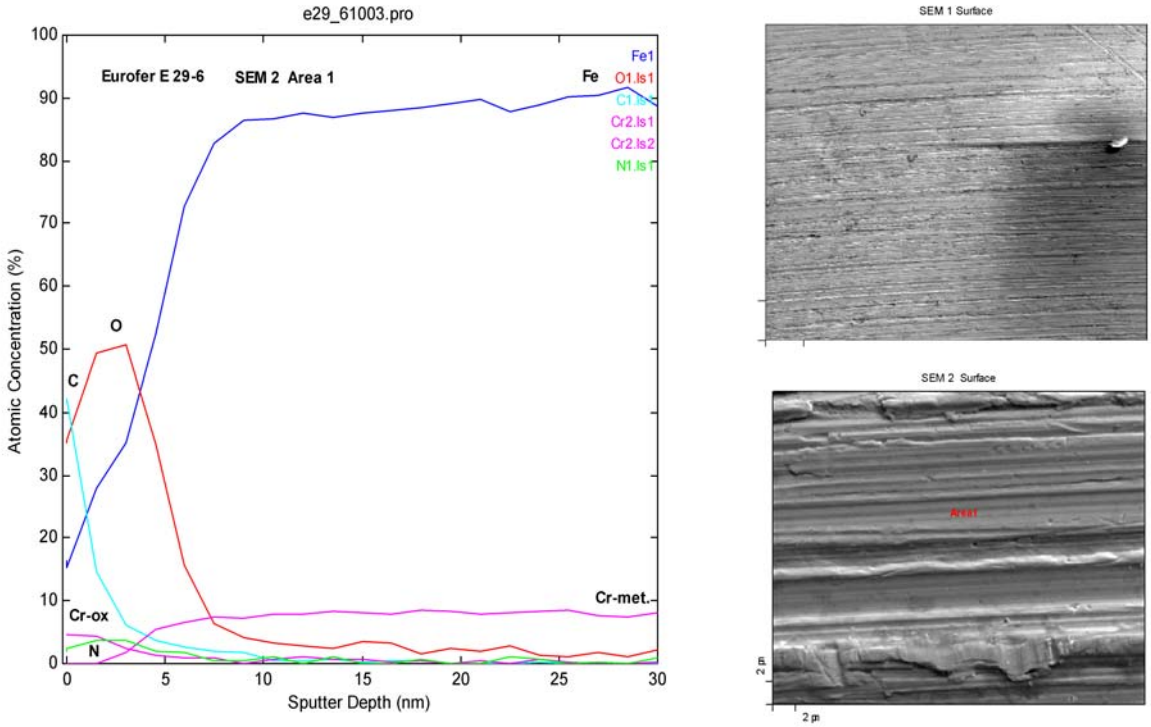

Fig. 5: Concentration profiles of C, N, and O for analyzed EUROFER surface. Left: SEM pictures of tested surface area.

3 Corrosion testing of Eurofer:

3.1 Metallographic analyses

In general, the observed mechanisms and phenomena known from 480°C tests are also valid and confirmed by the analyses of the Eurofer samples exposed at 550°C. For long exposure times a homogeneous dissolution of the steel is present. However, incubation times are shorter and corrosion attack is stronger. Some pictures will be given in this paragraph to illustrate the corrosion behavior vs. exposure time.

The analyses of the first removed sample exposed for 500 h indicate (Fig. 6), that the earlier during 480°C tests observed incubation times – were no corrosive attack was detected – is reduced to a level of smaller 500 h at 550°C compared to about 1,500 h for the 480°C tests. The metallographic examination of the 500 h sample showed a strong corrosion attack compared to the 480°C tests with an erosion depth in the range of 40 µm. Only some isolated areas were not attacked and allowed a simple and direct determination of the corrosion attack as selected in Fig. 6. The other parts of the surface – about 95 % of the circumference - showed already the homogeneous attack. A similar position with such a step was also found at the sample exposed for 1,025 h which allowed the direct measurement. Fig. 7 shows this position for the sample exposed for 1,025 h. The extrapolation of these both corrosion rates would yield in a rate of about 700 µm/a. After changing the magnetic trap due blockage by precipitations at about 2,500 h operation time a control sample, which was freshly installed, was additionally removed to the original plan for sample removal with an exposure time of about 500 h. This sample showed similar behavior compared to the first removed sample at 500 h. Wetting and corrosion attack is visible at about 95 % of the surface. The depicted area in Fig. 8 also allowed the direct detection of the

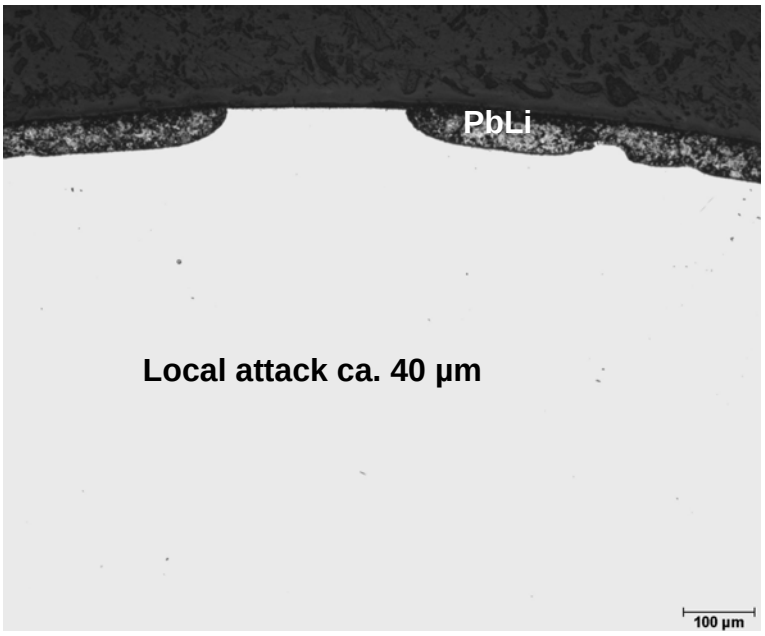

Fig. 6: EUROFER sample exposed to Pb-17Li at 550°C with attacked and unattacked surface.

corrosion attack by measuring the step height. For this sample the extrapolated corrosion rate would be near 630 µm/a. This control sample confirms that corrosion rates are strongly higher compared to the 480°C tests by obvious effects of steps on the surface and that the detected values have reliability in general and is not occasionally. The other 95 % of the surface shows a similar surface structure as depicted in Fig. 9 found at a representative sample exposed for long time (4,006 h) in this test series. This micrograph showed due to the smooth boundary line matrix – Pb-17Li scale also that dissolution is present and that no 'particles' are eroded.

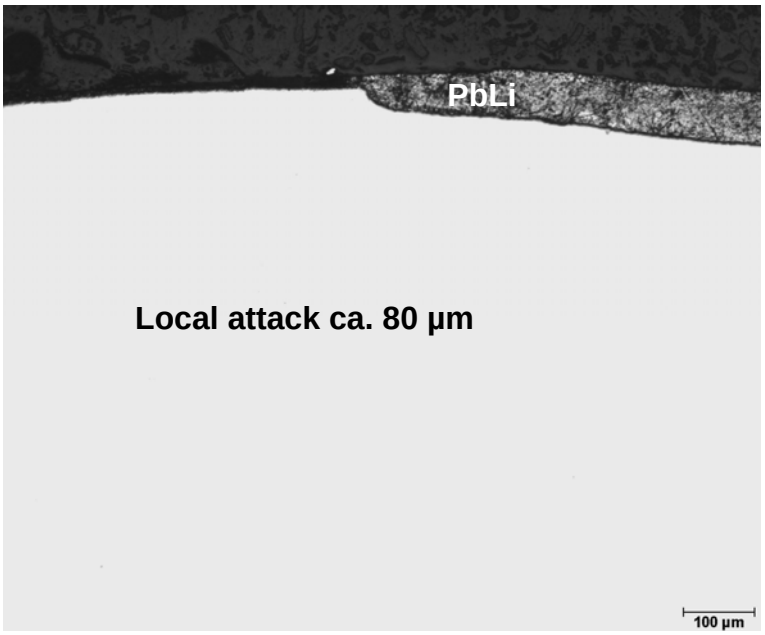

Fig. 7: EUROFER sample exposed to Pb-17Li at 550°C for 1,025 h with attacked and unattacked surface fraction

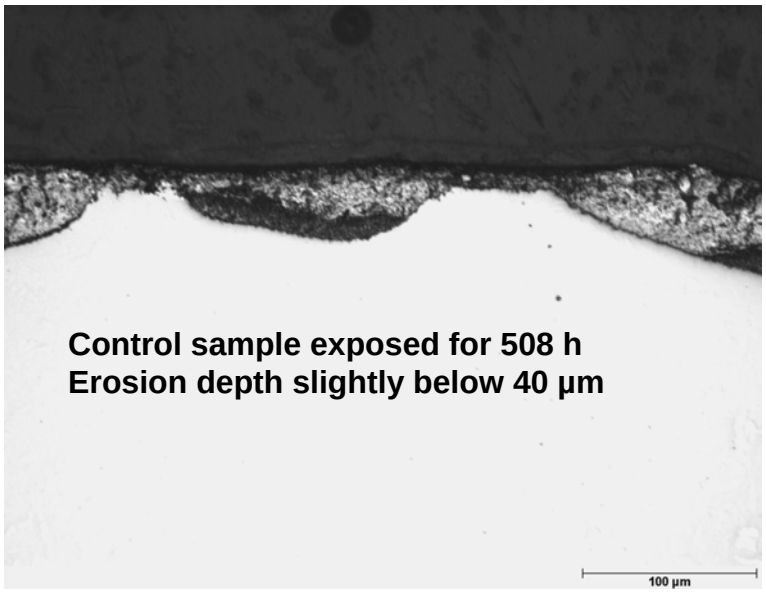

Fig. 8: EUROFER sample exposed to Pb-17Li at 550°C for 508 h during operation time from approximately 2,500 to 3,000 h.

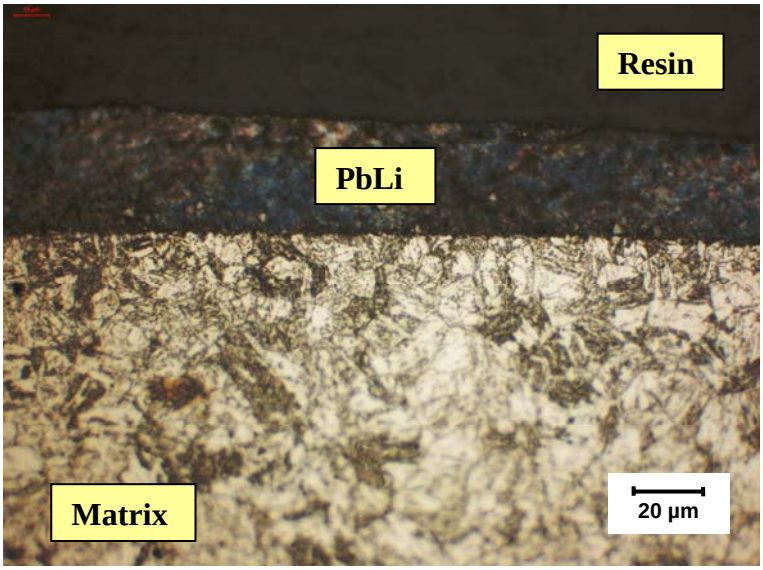

Fig.9: Sample exposed for ca. 4,000 h with adherent Pb-17Li scale and smooth surface indicating a homogeneous corrosion attack.

3.2 Determination of corrosion rate

Corrosion rates were evaluated for all exposed samples by a difference method by measurement of the diameters before inserting (fresh sample) and determination of the diameter after exposure. The latter values were measured using the micro-cuts prepared for metallurgical analyses as specified in more detail in [2]. This optical method was calibrated vs. a fresh reference sample with 'mechanically' determined diameter in the µm range. Additionally to these measurements of diameters the detected step height for short time exposed samples (500 and 1,000 h) was used to obtain a most reliable rate of corrosion attack. Fig. 10 shows the corrosion rate vs. time for the samples exposed to Pb-17Li with a flow rate of 0.22 m/s (target value) at 550°C.

The samples removed at 500 and 1,000 h exposure time to flowing Pb-17Li showed a rather strong corrosion attack. Both test methods measurement of step height and diameter reduction delivered the same result. The corrosion attack was homogeneous on the circumference of the analyzed cut position and no formation of an ellipsoid like shape was observed. The extrapolation to 1 year results in a corrosion rate of about 700 µm/a.

In contrast to these short time exposed samples a smaller corrosion attack was found for the samples exposed more than 1,500 h. Considering only the 5,000 h sample for long term extrapolation a corrosion rate of about 400 µm/a would be present. This value seems to be rather optimistic for predictions of life times. The evaluation of the whole test series favors a higher corrosion rate of about 500 µm/a as a more reliable one. The first test results at 550°C in the range up to 5,000 h testing time showed also a linear correlation for corrosion attack vs. time as known from the 480°C tests.

However, the diagram indicates that there is a large uncertainty in extrapolation to long term corrosion rates due to the short testing times. Meanwhile a new test series is under planning to enlarge exposure times to 10,000 h to provide a data base similar to the 480°C test series performed in the past.

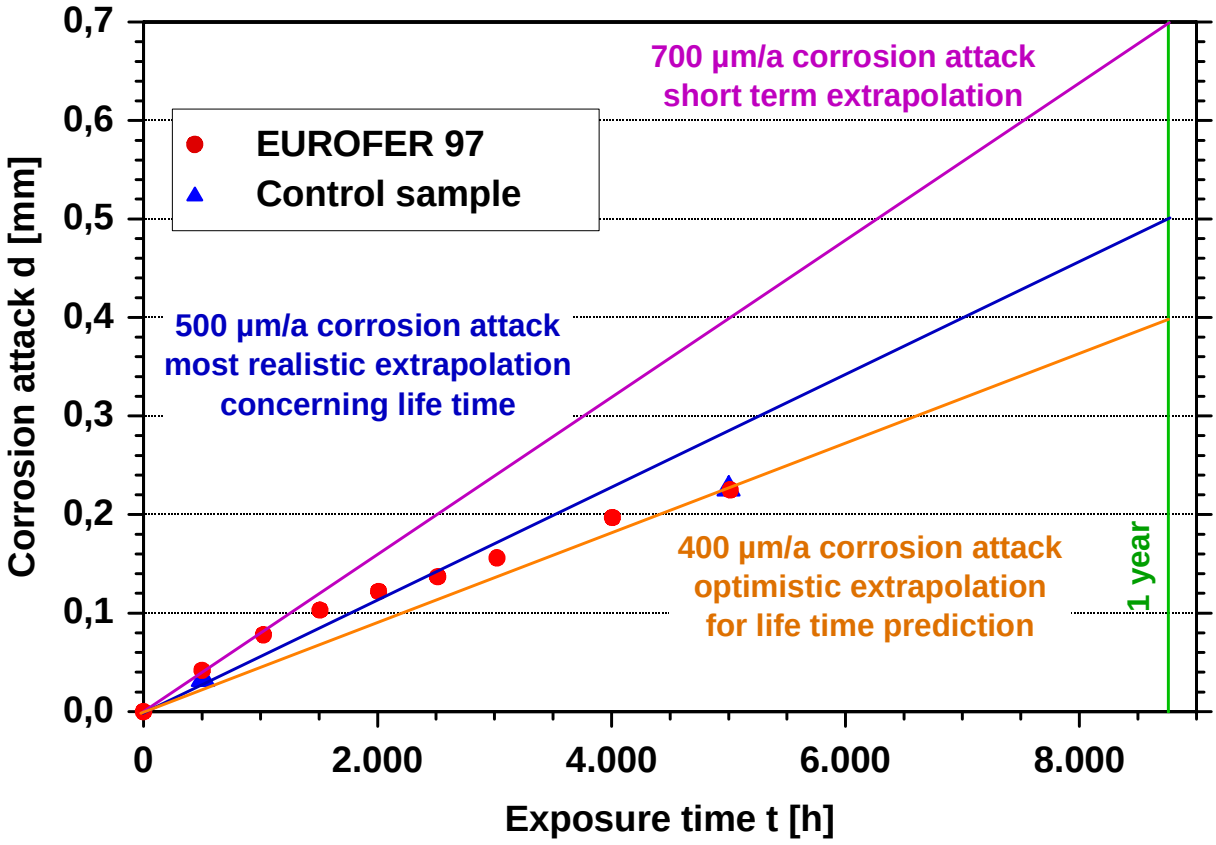

Fig. 10: Corrosion attack of EUROFER 97 samples at 550°C in PICOLO loop

3.3 EDX analyses

The performed micro structural analyses and the EDX measurements showed that no Pb diffusion into the matrix is present. Fig. 11 depicts optical and REM pictures of one EDX measurement position at the sample removed after 1,025 h from PICOLO loop. At the analyzed position the adherent PbLi scale had a thickness of about 40 µm. The concentration profiles are shown in Fig. 12. The Pb and Fe signals indicate that a sharp boundary line is existing between matrix and Pb-17Li. The EDX signals dropped sharply e.g. for Fe from about 90 % to zero in a small range of about 3 µm. This dimension of 3 µm is caused due to resolution effects (focus of the beam) and do not contradict a sharp drop. In the matrix the concentrations were constant and fit well to the Eurofer values determined by chemical methods. The given O-concentration is correlated to the formation of PbO scales on the micro-cuts and shows clearly the boundary between resin and adherent PbLi scale. This profile drops at the boundary to the steel also to zero and confirms so indirectly the sharp boundary between Pb-17Li and steel.

In the adherent Pb-17Li scale all analyzed steel elements showed an increased amount concerning their solubility limits in the liquid metal. Specially the elements with low solubility e.g. W have a similar concentration in the PbLi-scale compared to the Eurofer bulk. These values may indicate that a well mixing may not be present of the components in the reaction zone with the flowing PbLi bulk. Thus mixed transport phenomena (convection, diffusion) may be present in a small boundary or intermediate zone.

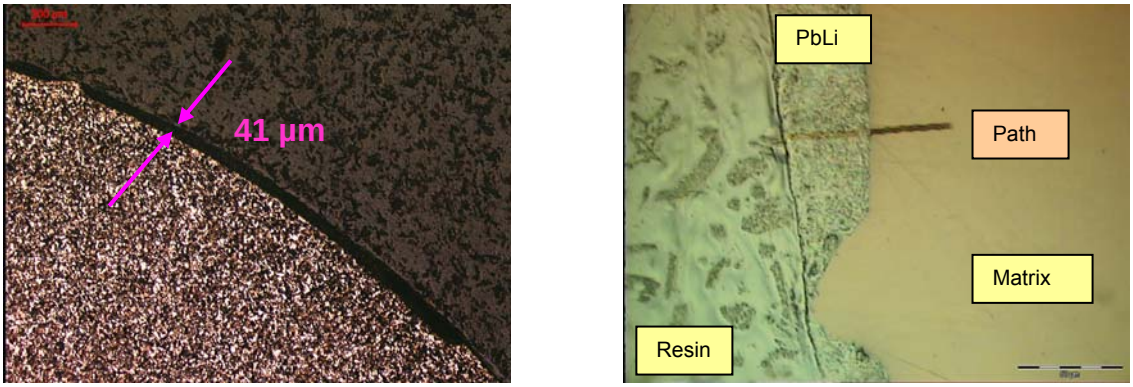

Fig. 11: Position of EDX analyses of sample exposed 1,025 h to Pb-17Li with a corrosion attack of about 41 µm. The REM-picture on the right side shows the eroded scan track.

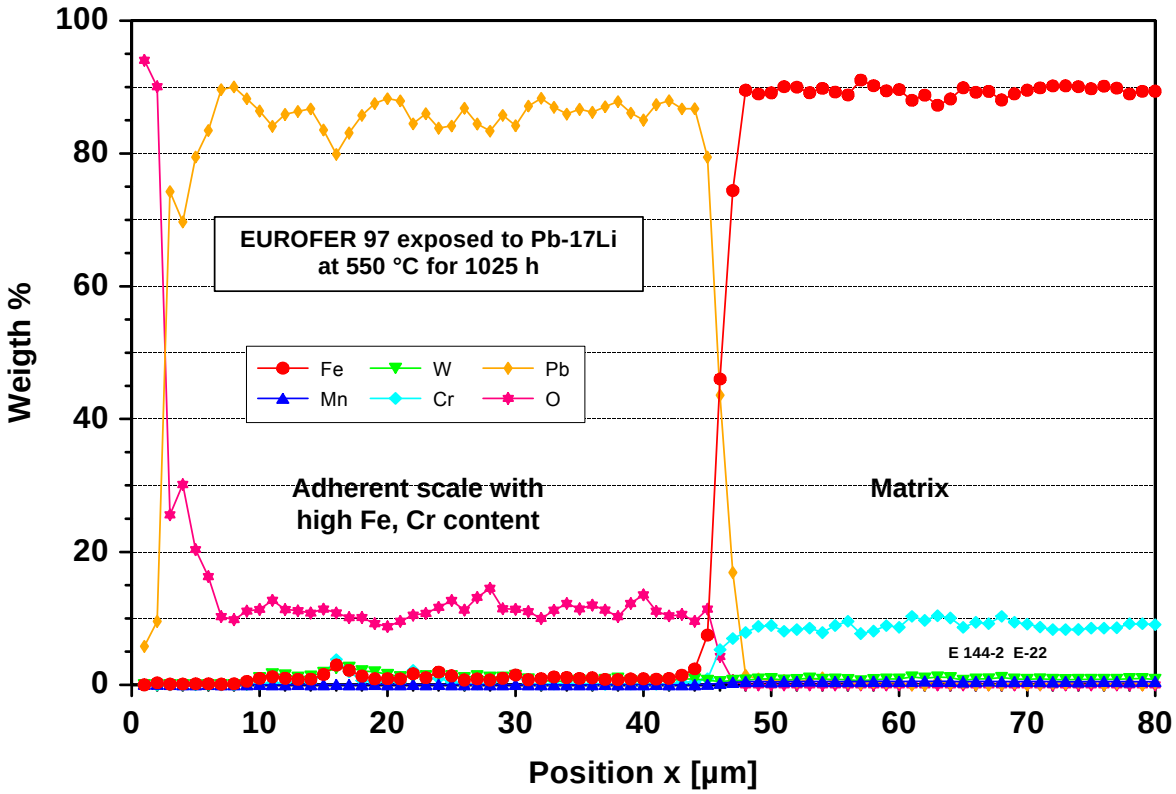

Fig. 12: EDX analyses of corrosion zone with adherent Pb-17Li scale as shown in micrographs of Fig. 11.

3.4 Comparison of 480°C and 550°C tests.

Under this task the corrosion behavior was analyzed for the first time in PICOLO loop at the elevated test temperature of 550°C for any steel. Thus a cross check - without modeling tools - of the measured corrosion rates of Eurofer with other steels is not possible as done in earlier tasks at 480°C to validate the reliability of the determined rates.

Thus Sannier's [4] corrosion correlation was used to get a feeling for the reliability of the measured 550°C rates. Of course this is an empirical correlation based on a lot of data coming from different test facilities and will have risks and will not replace modeling tools using physical parameters. However, several uncertainties will be reduced if only the parameter temperature is varied as valid for comparing the 480°C tests with the new 550°C values at the same flow rate of 0.22 m/s in PICOLO loop. Fig. 13 depicts the calculated metal loss in dependence of temperature for three flow rates a) the flow rate of 0.22 m/s used in PICOLO loop tests and b) two smaller flow rates of 0.05 and 0.005 m/s, respectively, to illustrate also the dependence on flow velocity. For the envisaged temperature of 550°C as new operation condition in TBM's calculated corrosion values are included. The two experimentally determined corrosion rates in PICOLO loop tests at 480 and 550°C with about 90 µm/a and 500 µm/a are a little bit smaller than the calculated values (127 µm/a and 553 µm/a) using the Sannier correlation.

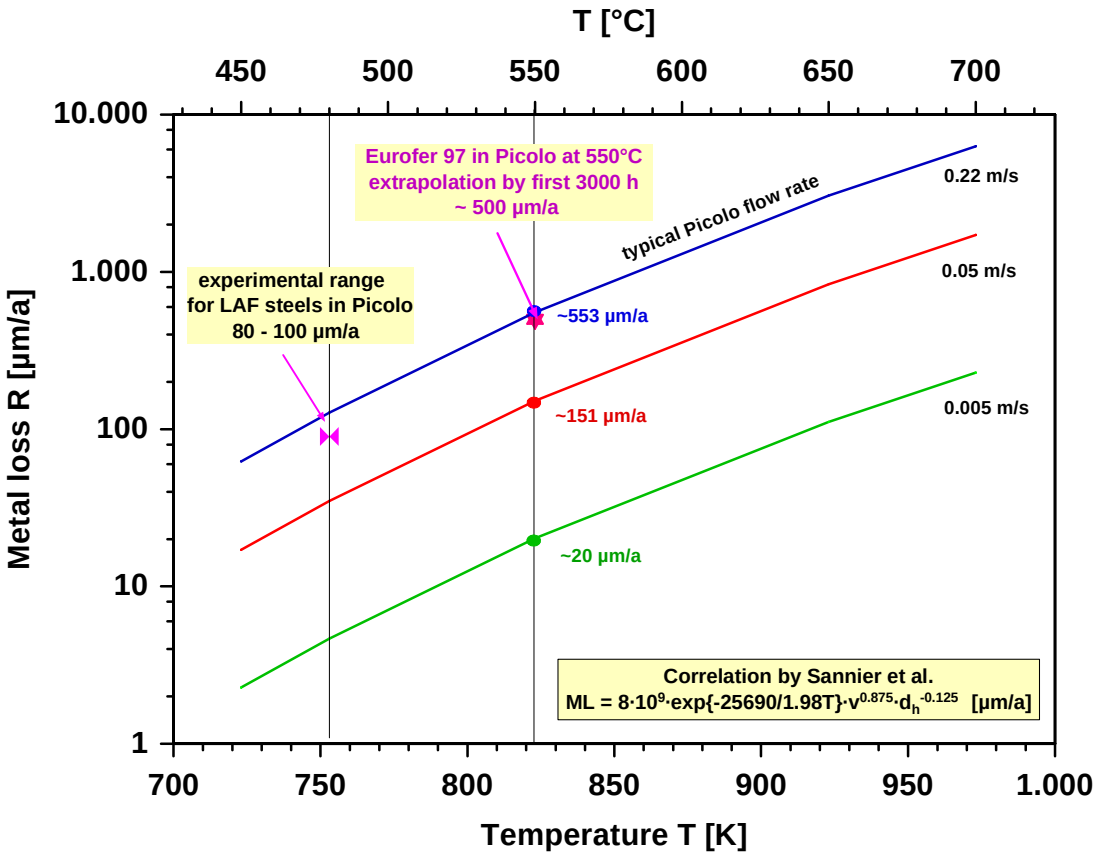

Fig. 13: Corrosion attack of RAFM steels is given using Sannier's correlation in dependence of temperature and flow velocity. Both values of PICOLO testing (480°C and 550°C) are included into the diagram.

This graphical illustration shows that the evaluated corrosion rate of about 500 µm/a at 550°C on base of only short term tests fits well into this metal loss scenario. This indicates that a high reliability may be present that 500 µm/a will not have to be corrected strongly by long term tests up to about 10,000 h exposure time.

This diagram confirms also that the found drastically increase in corrosion rate – by a factor of at least 5 - by enhancing the loop test temperature from 480 to 550°C – only 70 K higher – is real and not only a PICOLO phenomena. The diagram illustrates additionally that corrosion will be also at lower flow rates – more TBM relevant ones – still a serious process and will not disappear or reduce to a negligible value.

4. Precipitation effects

PICOLO loop is a closed loop testing facility with high temperature differences between test section and the cooler support components similar to general TBM conditions. In the past testing series at 480°C corrosion attack of RAFM steels was analyzed, however, the effects of transport of corrosion products and of there precipitation behavior were not investigated. A magnetic trap device was installed since the first tests were performed to prevent sensitive components by transported corrosion products and from their deposition. During the whole loop operation of more than 120,000 h at 480°C a loop blockage was rather seldom due to particle deposition in the magnetic trap. Thus, only a limited amount of changed components is available for re-evaluation of earlier tests.

4.1 Analyses of tube walls

Fig. 14 shows roughly the position of an analyzed tube section with respect to precipitations. This section was cut off from the loop after an operation time of about 77,000 h and had seen a temperature of about 380°C during normal operation. The switch off conditions at that moment was:

a) draining of the warm loop
b) natural cooling down to room temperature

The relevant cooling down time to the eutectic temperature of 235°C is estimated to be about 3 h and room temperature was reached over night.

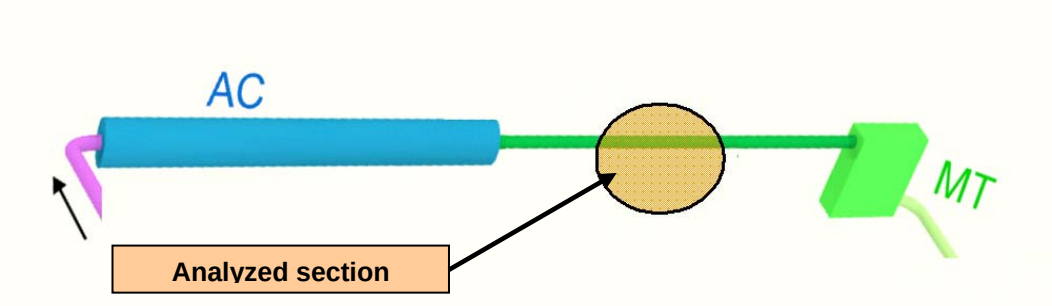

Fig. 14: Position of analyzed loop section between air cooler (AC) and magnetic trap (MT). Tube material is 1.4571 steel.

Fig. 15 shows the surface near section of the analyzed loop part. A coating of the inner wall surface by precipitated Fe/Cr - the opposite of the dissolution process found in the hot zone – is not visible. However, the wall is covered after draining by a Pb-17Li scale with embedded precipitations in various shapes. The performed EDX scans (Fig. 16) confirm that the observed particles are formed from the steel components Fe and Cr.

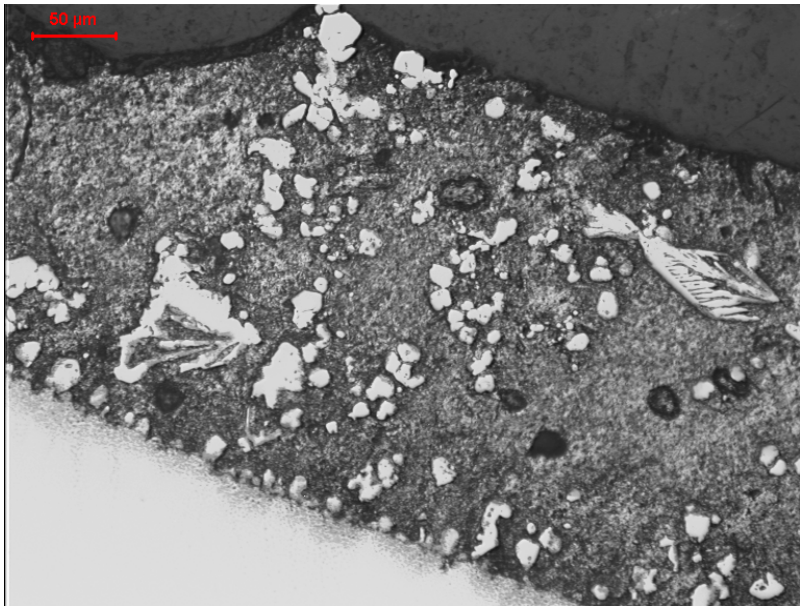

Fig. 15: Drained tube section with adherent PbLi scale

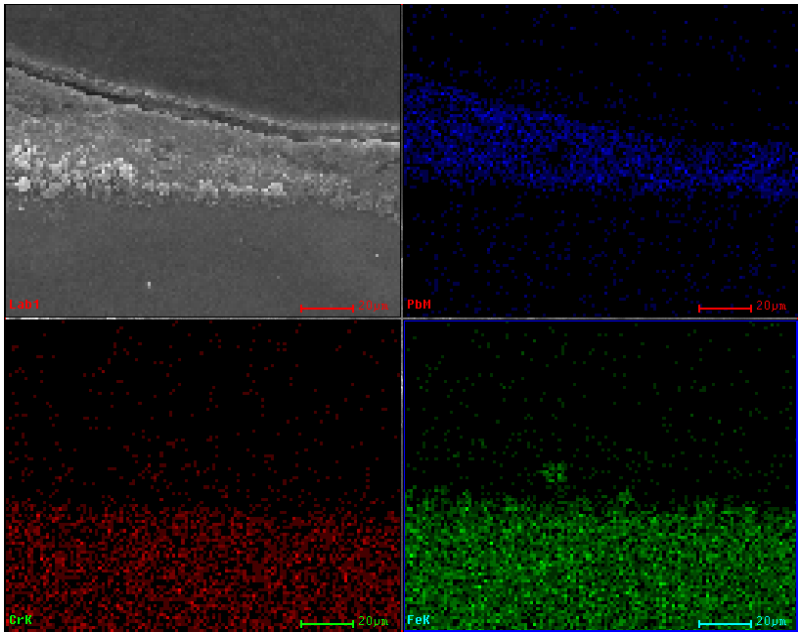

Fig. 16: REM and EDX pictures (element scans Pb, Cr and Fe) of analyzed tube section

A lot of these particles exhibit a rather filigree dendrite like structure as depicted in Fig. 17 with lengths of more than 100 µm. The large size indicates that they were not preliminary formed during the short time of cooling down. Both features no coating of the inner wall and the appearances of particles in the micro cuts confirm that precipitation effects take place as expected due to over-saturation of the melt. The performed analyses can not give hints to the loop position where the precipitations were grown and the amount of precipitated material. The large size of the particles

Fig. 17: Precipitations in adherent Pb-17Li scale

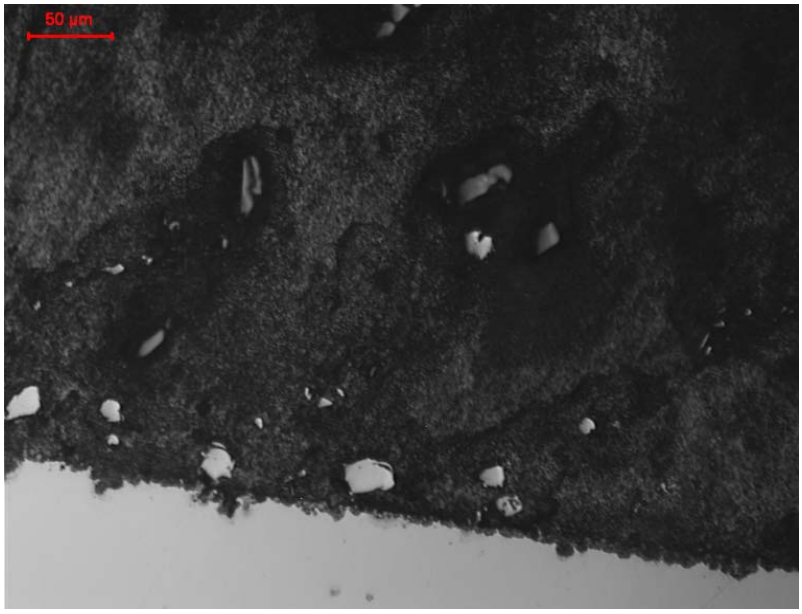

Fig. 18: Surface near position of PbLi in magnetic trap – inlet position

seen in the surface near area (Fig. 15) may raise speculations that the flow velocity is reduced in the surface near region and that viscosity may change with solute components. The metallurgical analyses of the magnetic trap and also the effect of loop blockage after about 3,000 h confirm that precipitated particles are transported. The series of figures with numbers Fig. 18, Fig. 19 and Fig. 20 shows analyzed positions in the magnetic trap. The highest amount of precipitations was detected in the centre of the trap where the magnetic field is strongest and the flow velocity is small. The dominant shape of the particles is dendrite like. The optical impression that a high concentration is present could not be confirmed by chemical analyses. They gave only values of some percents for Fe/Cr precipitations present in PbLi. The explanation is that they are arranged in a 3-dim. net which is able to block the loop section quickly as observed.

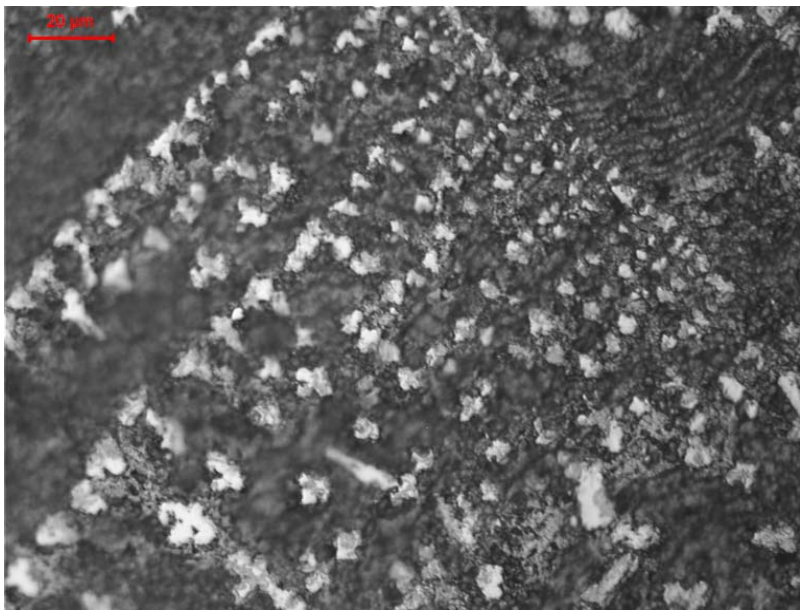

Fig. 19: Precipitations in the centre of the magnetic trap

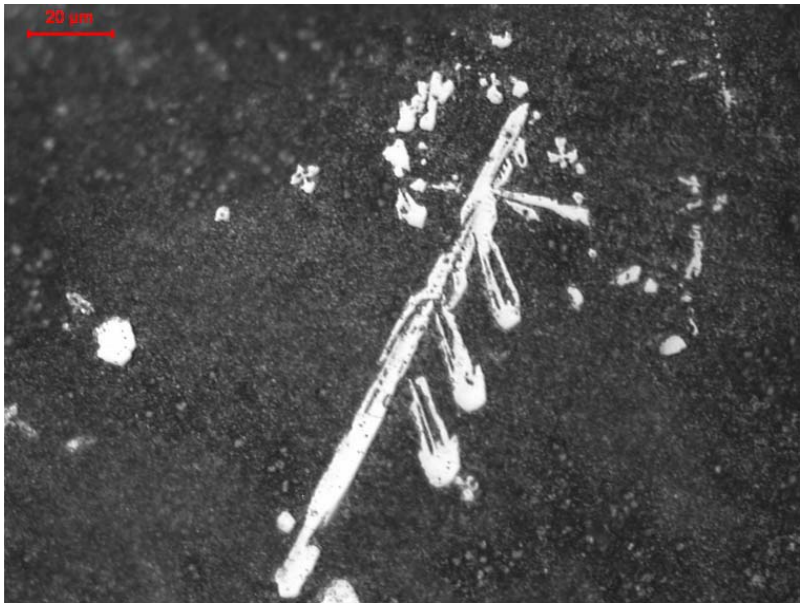

Fig. 20: Precipitation in magnetic trap outlet position

5 Impact of flow conditions in PICOLO tests on corrosion rate

5.1 Flow velocity

The analyses of the corrosion attack showed that with longer exposure time a smaller material take-off per time unit was observed / evaluated. However, the Fig. 10 corrosion attack vs. time implies that all parameters are constant during testing e.g. constant flow velocity. Under these assumptions such an interpretation would be correct, however, Fig. 13 (corrosion attack calculated by Sannier's correlation) shows clearly that with decreasing flow velocity material take-off will be smaller. The tests started with a flow velocity of about 0.22 m/s a value calculated from the mass flow (120 l/h) and the gap width between sample and tube wall. The tube diameter was 16.0 mm and the sample diameter was measured to be 8.0 mm thus the flow channel has a width of about 4.0 mm. Sample and tube material are rather similar and corrosion attack will take place at both parts and increase the gap width over time. Fig. 21 shows the effect of corrosion attack on flow velocity in PICOLO tests. As can be seen the flow velocity decreases significantly to about 0.175 m/s after one year or to roughly 0.195 m/s after 5,000 h from originally 0.22 m/s due to the strong increase of the gap area between sample and tube wall. This means that in the actual test series, a ca.10 % smaller flow rate was present after 5,000 h.

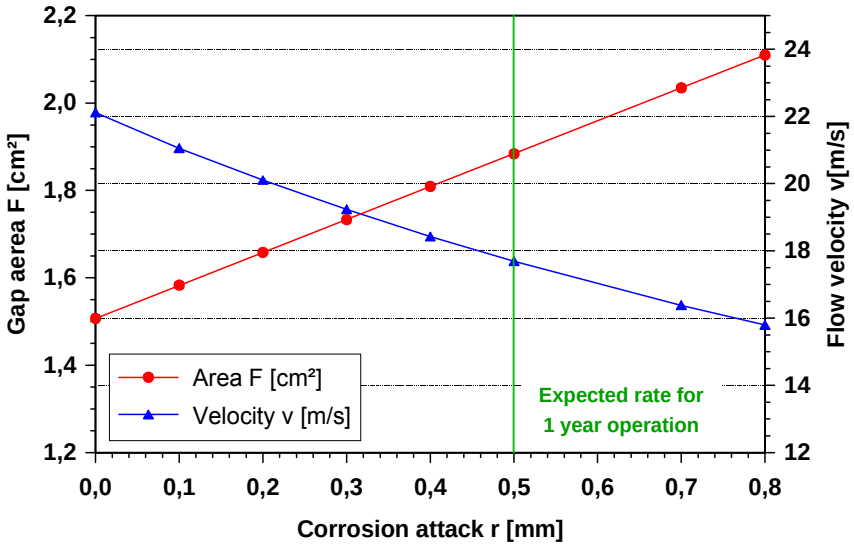

Fig. 21: Reduction of flow velocity and increase of PbLi gap vs. material take off

Under these test conditions the evaluated corrosion rates as depicted in Fig. 10 are too small and have to be corrected for constant flow velocity 0.22 m/s. Assuming that Sannier's correlation is valid at least for constant temperature and small changes in flow velocity a correction should be possible with high reliability. Sannier's correlation predicts material loss (ML) by:

$$ML = 8 * 10^{8} * \exp[-25690/1.98T] * v^{0.875} * d_h^{-0.125} \quad [\mu m/a]$$

Thus, the correction has to consider only the parameters v and d_h to find out relative changes. Fig. 22 shows the changes of $F(v*d_h)$ and the relative decrease compared to the value F_0 for v_0 = 0.22 m/s and d_{h0} = 4.0 mm in dependence of corrosion attack.

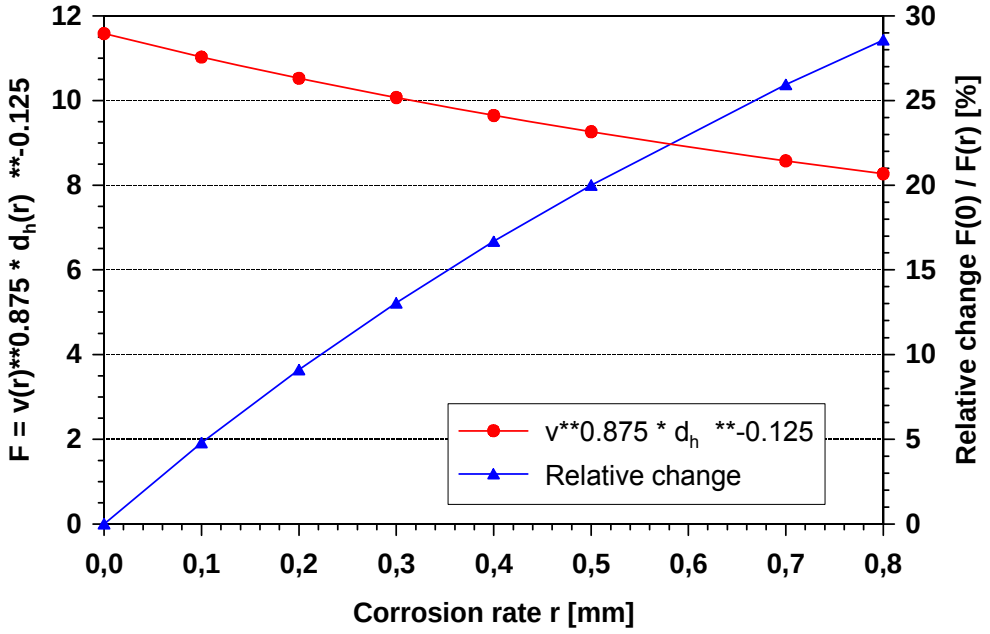

Fig. 22: Reduction of corrosion attack compared to v_0 = 0.22 m/s and d_{h0} = 4.0 mm

For a material loss of about 0.25 mm – similar to the value determined for exposure time 5,000 h in PICOLO loop – a reduced corrosion attack by about 12 % is predicted if these loop parameters would be used for the test series. Assuming that the correction factor F(0)/F(r) changes linearly all observed rates have to be increased e.g. the measured value for 5,000 h by 0.5 * 12 % = 6 %.

5.2 Other parameters

Beyond the dimensional changes due to corrosion in the test section other loop parameters will also have an impact on the corrosion rate e.g. the mass flow. The mass flow was measured during the whole corrosion testing and the pumping power was adjusted to keep the designed mass flow nearly constant. For most of the testing time the mass flow was between about 110 and 120 l/h. Only under certain conditions e.g. before changing the magnetic trap the mass flow dropped to values near 90 l/h for some hours. Analyzing the whole test duration of 5,000 h the smallest deviation from the projected mass flow of about 120 l/h was present in the beginning of the testing up to about 1,500 h. Later on e.g. precipitation effects caused more and stronger pumping power adjustments. Under normal condition – fare away from loop blockage – the control system went into operation at a minimum mass flow near 110 l/h. This characteristic in mass flow control and mass flow behavior leads also to smaller corrosion attack at longer exposure times similar to the increase in gap width. The total operation times with smaller mass flow – down to the 90 % value - were evaluated to about 600 h in sum. The reduction of 10 % in mass flow reduces the flow rate to about 0.195 m/s – the same value as calculated for larger gaps due to corrosion. However, the total time base is smaller by roughly a factor 10. Thus the expected effect should not exceed the 1 % range. Fig. 23 shows the corrosion attack vs. expose time for both all measured and two corrected data points for 4,000 and 5,000 h exposure time.

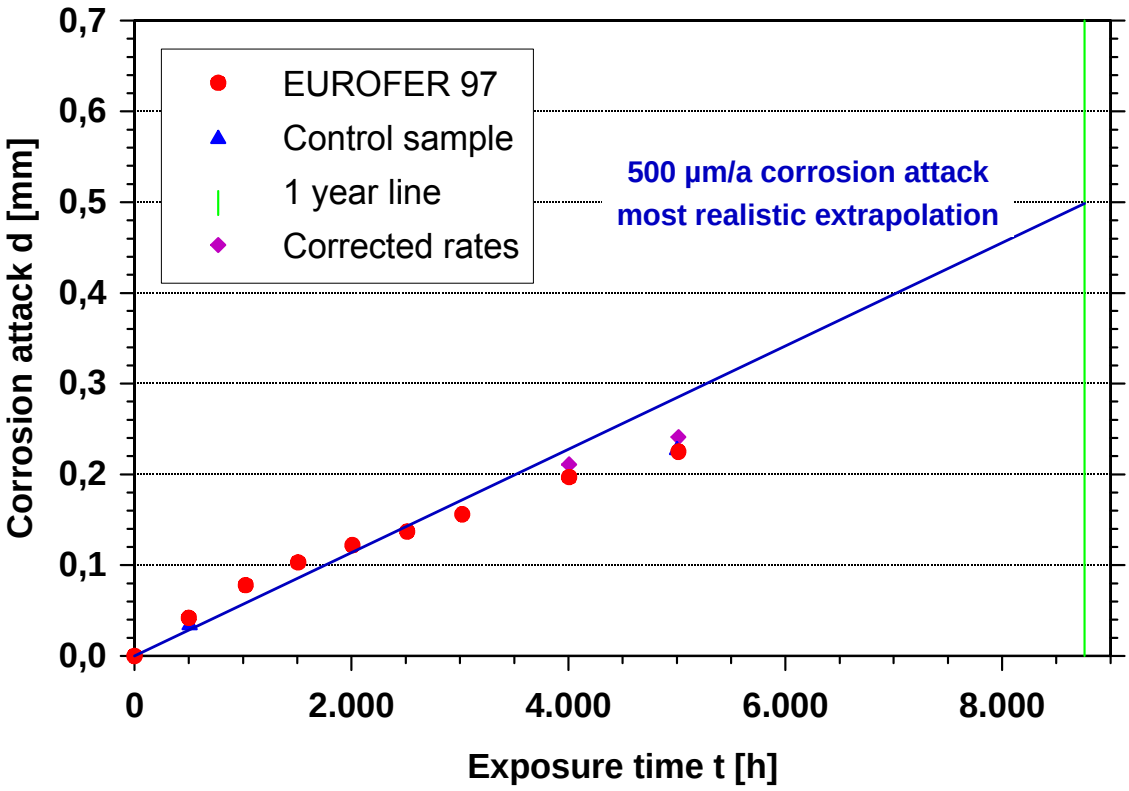

Fig. 23: Measured corrosion attack and corrected values to constant 0.22 m/s flow velocity in test section

Such discussions of a possible impact of the behavior of loop parameters will only affect the part extrapolations to long term corrosion behavior and not the quality of the measured data. As illustrated above these special effects during testing e.g. a decrease of mass flow or gap widening due to corrosion vs. exposure time will lead to too optimistic corrosion rates under long term view for TBM's if only selected samples are considered and test conditions change. To eliminate or at least to reduce such singular effects the testing program is meanwhile extended to 10,000 h.

6 Remarks

PICOLO loop was upgraded for working at the new test temperature of 550°C and the test campaign reached the proposed duration of 5,000 h successfully. The evaluated corrosion rate for 550°C is drastically increased to about 500 µm/a compared to a value of 90 µm/a detected in 480°C tests. The performed cross check of the evaluated 500 µm/a corrosion rate confirms this number as a realistic value considering that Eurofer was tested for the first time at 550°C and only some data points are available without statistics and any possibilities in comparing test series as known from the 480°C testing of different steel types. Looking on transport and precipitation effects first data were collected. At the moment it seems that more questions were generated considering e.g. the assumption that transported corrosion product will be mostly deposited on the inner wall surfaces at the cooler sections. This high corrosion value and the feature of loop blockages after only 3,000 h operation time at 550°C illustrate that corrosion attack and transport phenomena will be serious tasks looking towards TBM's. The resume of this testing campaign and their evaluation is that reliability of the extrapolated corrosion attack for long terms has to be increased with enlarging the testing base to about 10,000 h. Beyond this 'corrosion testing at v = .22 m/s' additional data points at smaller flow velocities are required to confirm the corrosion puzzle of corrosion attack vs. temperature and flow rate and to validate modeling. These tasks look more straight forward compared questions transport and precipitation phenomena. Of course, this topic is included in the newly started TW6 task, however, the relevance and the required resources are valued not correctly at the moment to solve these difficult and time consuming processes. The given first results may rice the priority in looking on precipitations.

B. Model development

1 Introduction

The Pb-17Li alloy is considered as a liquid breeder in future fusion reactors. One major problem in non-isothermal liquid metal systems lies in the corrosion of their structural materials, consisting mainly of martensitic and austenitic stainless steels. It is generally accepted that corrosion of steel components in flowing liquid Pb-17Li is only ruled by dissolution processes. Although Pb-17Li loops are operated with low oxygen concentrations preventing the formation of new oxide phases, we must foresee existing oxide scales or other protective layers on structural components. The locations of dissolution and precipitation are mainly determined by the temperature dependence of the solubility of the metal alloys if no oxide scale is present. This means that we have dissolution in the hot parts of the system and precipitation in the cold parts, irrespective of the nature of the dissolution process, whether it is exothermic or endothermic.

Precipitation of clad material at cooler parts of the system can have consequences as there may be clogging and plugging of components having small cross sections. This may also affect maintenance and repair of the system as in a Fusion reactor there will be activation of steel components and there will be a transport of activated material. We have developed a simple model, which calculates the mass transfer and the geometrical changes of structural components in liquid metal loops. This model was implemented in the computer code MATLIM.

2 Theoretical background

In general, one has forced convection flow conditions in liquid metal loops, either laminar or turbulent flow. If one wants to calculate the transport of ions, atoms, or molecules present in the liquid metal in a certain concentration c_i (with i denoting the solute), one can use the convective diffusion equation (cp. ref. [5]):

$$\frac{\partial c_i}{\partial t} + (\vec{v}\nabla)c_i = \nabla(D_i \nabla c_i) \qquad (1)$$

where $\vec{v}$ is the velocity of the liquid metal and D_i the diffusivity of solute i in the liquid metal.

The convective diffusion equation is given in its most general form, assuming that the concentration can depend on the axial position x in the loop and on transversal coordinates and that there can be a transient phase. Such a procedure has been adopted by Zhang and Li, which have published a series of papers [5 - 9]. But one can also take a different route for the solution of the problem. Namely, one can take profit of the principles of convective mass transfer, which stipulate that under forced convection flow conditions the mass flux is determined by a dimensionless characteristic flow parameter, the so-called Sherwood number; and we can take profit (if needed) of the analogy between heat and mass transfer.

Thus, the mass flux of the solute i from the channel wall into the bulk of the fluid is given by the following equation (cp. ref. [12]):

$$j_i = K_i^{fl} \cdot (c_i^w - c_i^b) \tag{2}$$

where K_i^{fl} is the mass transfer coefficient for the solute *i*, c_i^w the concentration of the solute *i* at the wall and c_i^b is the concentration in the bulk of the fluid.

The direction of the mass flux depends on the ratio of the two concentration values. If c_i^w is higher than c_i^b then the mass flux is directed from the wall into the fluid; if c_i^w is smaller than c_i^b then the mass flux is directed from the fluid to the wall. In the following we make implicitly use of the fact that the solutions of the thermo hydraulic equations depend on characteristic non-dimensional quantities, which is finally a consequence of Buckingham's Π-theorem [10].

The mass transfer coefficient K_i^{fl} is determined by the Sherwood number Sh in the following way:

$$K_i^{fl} = \frac{D_i}{d_{hyd}} \cdot Sh \tag{3}$$

where d_{hyd} is the hydraulic diameter.

Bringing the convective diffusion equation (1) into a non-dimensional form, one can show that under forced convection flow conditions its solutions depend on the Reynolds number Re and on the Schmidt number Sc. Thus, the Sherwood number Sh, which is the characteristic number for the non-dimensional mass flux, must also depend on the Reynolds number and on the Schmidt number. Therefore we have the following functional relationship:

$$Sh = a \cdot Re^{\alpha} \cdot Sc^{\beta} \tag{4}$$

The parameters *a* and α, β must be determined experimentally depending on the flow regime.

$$Re = \frac{u_{fl} \cdot d_{hyd}}{\upsilon_{fl}} \qquad Sc = \frac{\upsilon_{fl}}{D_i} \tag{5}$$

where υ_{fl} is the kinematic viscosity of the fluid and u_{fl} the flow velocity.

It remains to calculate the solute concentration in the bulk of the fluid c_i^b along the whole loop. This is done with the help of the mass conservation law. In this way we have derived the following differential equation:

$$\frac{\partial c_i^b(t,x)}{\partial t} + u_{fl} \cdot \frac{\partial c_i^b(t,x)}{\partial x} = \frac{U_{ch}}{A_{ch}} \cdot j_i(t,x) \tag{6}$$

where U_{ch} is the circumference of the flow channel, A_{ch} the cross section of the flow channel and u_{fl} the flow velocity in the coolant channel.

The axial position x in the loop is to be understood as a length of flow path, as the different axial sections of the loop are added in a scalar way irrespective of their orientation in space. There we have assumed that the bulk concentration does not depend on transverse coordinates, as the concentration c_i^b in the liquid metal is practically uniform, with appreciable concentration differences appearing only in a very thin layer at the wall. This thin layer was neglected in the derivation of eq. (6). We have also to fix the boundary conditions. In a closed loop we have the following periodic boundary condition:

$$c_i^b(t,0) = c_i^b(t,L) \tag{7}$$

where *L* is the total length of the loop.

In a pipe flow situation we would have in most cases the following condition at the inlet:

$$c_i^b(t,0) = c_i^0(t) \tag{8}$$

x = 0: axial position of the inlet.

If there is a magnetic trap at some axial location $x_{m.tr.}$, which is able to remove the magnetic solute i quantitatively we would also have:

$$c_i^b(t,x_{m.tr.}) = 0 \tag{9}$$

The value which we have to take for c_i^w depends on the nature of the interface. If the solute results from an interface reaction with a rate constant k_s we have a two step mechanism and the overall mass transfer coefficient K_t is given by [10]:

$$K_t = \frac{k_s \cdot K_i^{fl}}{k_s + K_i^{fl}} \tag{10}$$

When $k_s \gg K_i$ then $K_t \rightarrow K_i^{fl}$. We have also assumed that there is no diffusion surface layer, which the solute *i* must pass. Otherwise, the overall mass transfer coefficient is given by:

$$K_t = \frac{K_i^{fl} \cdot D_i^{s.l.}/\delta}{K_i^{fl} + D_i^{s.f.}/\delta} \tag{11}$$

where $D_i^{s.l.}$ is the diffusion coefficient of the species *i* in the surface layer and δ the thickness of the surface layer.

Using the overall mass transfer coefficient we have the following equation:

$$j_i = K_t \cdot (c_i^s - c_i^b) \tag{12}$$

with c_i^s being the solubility of the species *i* in the liquid metal.

3. Dissolution and precipitation rates

We have now all the necessary elements for the calculation of the dissolution and the precipitation rates, one of the main aims of this work. We are mainly concerned with stainless steel components and in the foregoing we will derive formulas relevant for this kind of material. If we have an existing oxide scale consisting of magnetite the dissolution and precipitation rates are given as:

$$b_{ox} = -j_{Fe} \cdot \frac{3 \cdot M_{Fe} + 4 \cdot M_O}{3 \cdot M_{Fe}} / \rho_{ox} \tag{13}$$

where j_{Fe} is the iron flux, M_i the atomic weight of the species i and ρ_{ox} the specific density of the magnetite.

If we have an iron-chromium spinel, the ratio of the atomic weights in eq. (13) has to be modified accordingly. We have adopted the convention that in case of dissolution the rate b^{ox} is negative and in case of precipitation positive. If there is no passive oxide present, the dissolution and precipitation rates depend on the behavior of all the alloying components. If f_{Fe} measures the mass fraction of all the alloying elements of the cladding dissolved or precipitated which can be attributed to iron, we get:

$$b_{me} = -j_{Fe} \cdot \frac{1}{\rho_{ss} \cdot f_{Fe}} \tag{14}$$

where ρ_{ss} is specific density of stainless steel.

It should be noted that in both cases the calculated iron flux which appears in eqs. (13) and (14) is very different, as the solubility can differ by order of magnitudes.

4 Stability of passive layers

If the concentration of oxygen in a liquid metal is above a certain limiting value, oxide scales can be formed on stainless steel components. We assume that in the absence of dissolution the increase of the oxide scale can be described by some function $r(T,c_O)$ for the oxidation rate and then we can establish the following balance equation for the oxide scale:

$$\frac{d\delta_{ox}(t)}{dt} = r(T,c_O) + b_{ox} \tag{15}$$

c_O: oxygen concentration in the liquid metal.

A similar equation has originally been used by Tedmon [11] for high-temperature oxidation with simultaneous volatilization of Cr_2O_3. If the liquid metal loop is operated at a very low oxygen concentration as is the case for Pb-17Li, **no** (new) oxide is formed and we obtain:

$$\frac{d\delta_{ox}(t)}{dt} = b_{ox} \tag{16}$$

In the high temperature region we have dissolution and b_{ox} is negative and the existing oxide scale is gradually dissolved at a constant rate b_{ox}. The so-called incubation phase is terminated at a certain axial location x, when the dissolution of the oxide scale is completed.

In a time increment Δt the inner channel wall radius will change by:

$$\Delta r_i^{ch} = -b_{ox} \cdot \Delta t \tag{17}$$

The sign convention is that in case of dissolution b_{ox} is negative and in case of precipitation it is positive.

If no oxide scale is present on the inner clad wall, we have in the dissolution and in the precipitation regime the following equation:

$$\Delta r_i^{ch} = -b_{me} \cdot \Delta t \tag{18}$$

In case of a low oxygen concentration in the liquid metal no oxide is precipitated and the rate b_{me} is to be applied to calculate the evolution of the inner channel wall in the precipitation regime.

5 Correlations for the mass transfer coefficient, for the solubility and diffusivity

The newly developed model has been incorporated in the computer code MATLIM, where the relevant differential equations are solved with the help of finite difference techniques by dividing the whole loop into a certain number of axial meshes. In the actual version of the code a value of 1,000 axial meshes is used. But this value can easily be increased if there is a need. In this way multi-modular loops can easily be treated, as specific values for the relevant parameters can be assigned for each axial mesh

There are mainly three different types of physical properties and parameters, which determine material behavior in a liquid metal system. The first group concerns the thermo-hydraulic data of the system like the flow velocity and the hydraulic diameter but also the temperature distribution along the system (Fig. 24). The second group concerns material data like viscosity of the liquid metal, diffusivity and solubility of the solutes. The third group encompasses properties of the wall materials itself. The dependence on the thermo-hydraulic parameters is evident from eqs. (3) and (4) and will be discussed in the following for turbulent and laminar flow conditions.

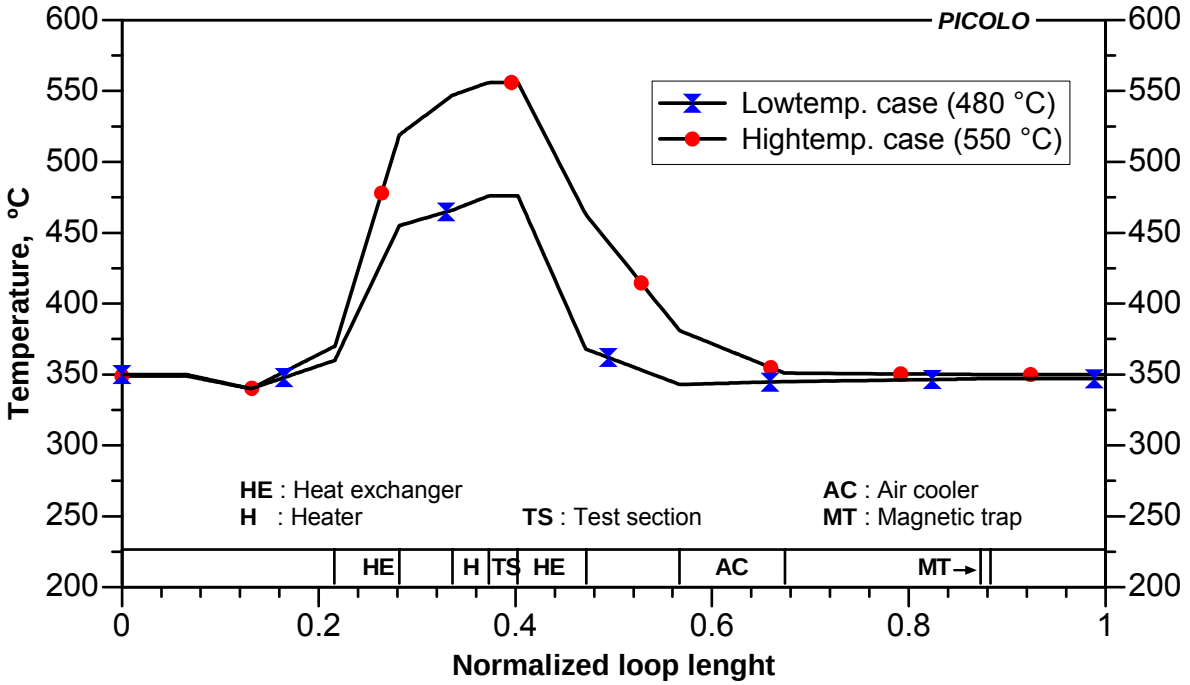

Fig. 24: Temperature distributions in the PICOLO loop (low and high temp. case)

There are a number of correlations for the mass transfer coefficient obtained under fully developed turbulent pipe flow. Our main assumption is that they can also be applied for liquid metal loops. Three of these correlations were investigated and discussed in ref. [12]. These are the correlation of Berger and Hau [13], that of Silverman [14], and that of Harriott and Hamilton [15]. The range of validity for the Berger and Hau correlation is for example given in ref. [12] as follows:

$$8 \cdot 10^3 \le Re \le 2 \cdot 10^5 \,,\; 1000 \le Sc \le 6000 \tag{19}$$

All these three correlations give similar values for the mass transfer coefficient. It is therefore sufficient for us to use only one of them, namely that of Silverman [14]:

$$K_{Silv} = 0.0177 \cdot u_{fl}^{0.875} \cdot D_{Fe}^{0.704} / (d_{hyd}^{0.125} \cdot \upsilon_{fl}^{0.567}) \tag{20}$$

In case of laminar flow we can make use of the analogy between heat and mass transfer. There is a lot of information on the heat transfer in pipe flow (laminar and turbulent, inlet flow or fully developed flow) in ref. [16], which can be applied to mass transfer by replacing the Nusselt number by the Sherwood number and the Prandtl number by the Schmidt number.

The model incorporated in the code MATLIM is flexible enough, as in each axial mesh of the loop we can specify the value of the mass transfer coefficient. We are not going to discuss this in all details but only give here the Sherwood number for small values of the parameter $Re \cdot Sc \cdot d_{hyd}/x$ (x = axial distance from the inlet) [16]:

In case of a full circular cross-section:

$$Sh_{la} = 3.66$$

In case of an annular cross-section [16]:

$$Sh_{la} = 3.66 + (4 - 0.102/(d_i/d_o + 0.02))(d_i/d_o)^{0.04} \quad (21)$$

where d_i , d_o are inner, outer diameter of the flow channel.

There we have made use of the analogy between heat and mass transfer, that means replaced the Nusselt number by the Sherwood number. We have applied the Nusselt number correlation given in [16] for fixed values of the wall temperature and not that for fixed values of the heat flux, as these values are to be transferred for a situation with fixed values for the concentration of the solutes at the wall. It should be noted that in case of fully developed laminar flow the mass transfer coefficient does not depend on the flow velocity and increases linearly with the iron diffusivity.

The flow in pipes is laminar up to a Reynolds number of 2,300 and it becomes fully turbulent at a Reynolds number of 10,000. In between we have a transition regime. In order to describe this transition regime we follow the procedure proposed in [16], which is based on a linear interpolation between the Nusselt numbers in the laminar and in the turbulent regime.

Defining the parameter γ as:

$$\gamma = \frac{Re - 2300}{10^4 - 2300} \quad (22)$$

we obtain the Sherwood number in the transition region as follows:

$$Sh_{tr} = (1-\gamma) \cdot Sh_{la}(2300) + \gamma \cdot Sh_{turb}(10^4) \quad (23)$$

Sh_{turb} is the Sherwood number in the fully turbulent region.

For Pb-Li, the following correlation for the iron solubility was given in ref. [12, 17, 18]:

$$c^s_{Fe}(T) = 10^{2.524 - 655.07/T} \text{ in wppm} \quad (24)$$

The solubility data in ref. [19, 20] on the other hand would give values lower by about a factor of 1000:

$$c^s_{Fe}(T) = 10^{10.733 - 9345/T} \text{ in wppm} \quad (25)$$

Coen et al. determined their correlation of the iron solubility by performing immersion tests determining the concentration of dissolved metal in the liquid alloy by atomic absorption spectroscopy. Borgstedt et al. deduced the iron solubility from dissolution tests in flowing Pb-17Li using a certain correlation for the mass transfer coefficient and certain values for the iron diffusivity (Sutherland-Einstein) and the Schmidt number. It should be noted that the solubility values of Borgstedt et al. are close to that in pure lead [20, 21].

The solubility of iron in Pb-17Li was also determined by Feuerstein et al. [22] by dissolution tests in crucibles. For tests done with alpha-Iron the following correlation has been obtained (Fig. 25):

$$c^{s}_{Fe}(T) = e^{4.94 - 4292/T} \quad \text{in wppm} \tag{26}$$

This correlation gives a value of about 1 wppm at 600°C, considerably lower than the values given by the correlation (24). In ref. [22] were also compared the solubility correlations of iron different authors and it was concluded that the values of Coen, Barker and Sample [17, 18] are too high.

Two data points for the iron solubility of stainless steels were also given in ref. [22] and from these two data points we have derived the following correlation (Fig. 25):

$$c^{ss}_{Fe}(T) = 1.1016E6 \cdot e^{-10389/T} \quad \text{in wppm} \tag{27}$$

At 600°C this correlation yields a value of about 7.5 wppm, distinctly higher than that for α-Iron.

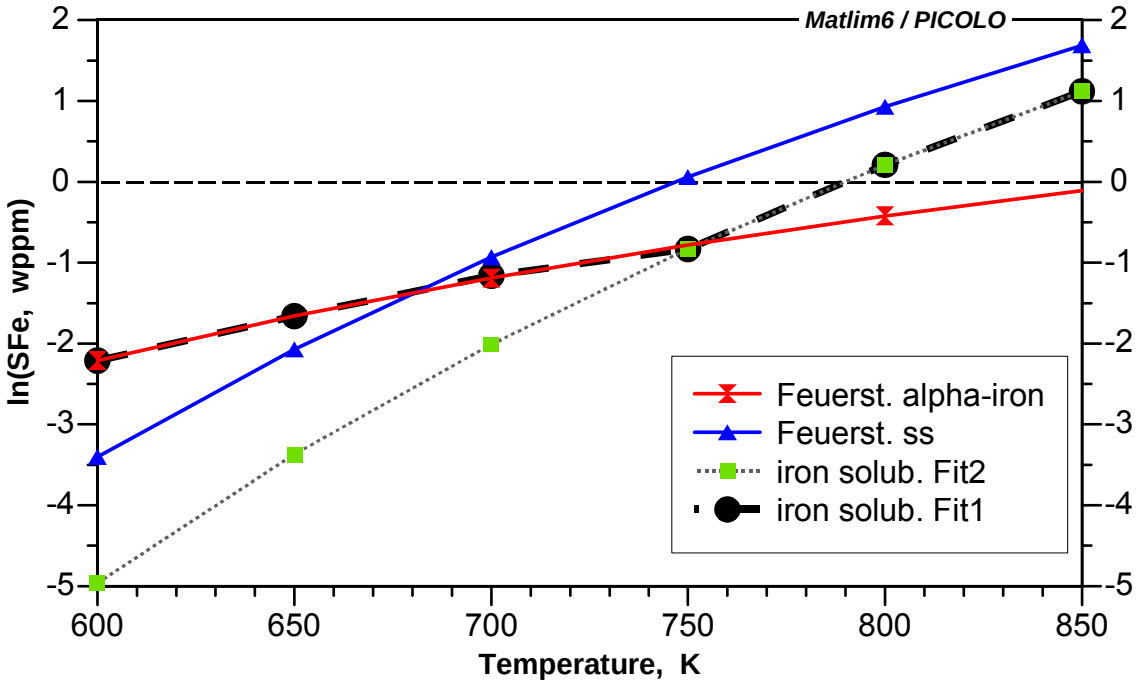

Fig. 25: Iron solubility in Pb-17Li versus temperature according to Feuerstein et al. [22] (α-Fe and ss) and according to proposed fits

The solubility of oxygen in Pb-17Li is discussed in [23]. Two values have been given in [24], namely $3 \cdot 10^{-3}$ wppm at 743 K and $1 \cdot 10^{-2}$ wppm at 823 K. With these two data points we have established the following provisional correlation for the oxygen solubility:

$$c_O^S(T) = e^{6.519 - \frac{9160}{T}} \text{ in wppm} \tag{28}$$

If there is an oxide scale present on the metallic surface the respective solubility correlation relevant for the oxide is to be applied. There are correlations for the solubility of magnetite in Pb and LBE to be found in the literature [5], but not for any oxides in Pb-17Li.

The diffusivity of single-atom solutes in liquid metals can be calculated with the help of the Sutherland-Einstein equation [5, 12]:

$$D_i(T) = \frac{k \cdot T}{4 \cdot \pi \cdot \eta_{fl}(T) \cdot r_i} \tag{29}$$

where η_{fl} is the dynamic viscosity of the fluid and r_i the atomic radius of the solute.

With an atomic radius of $1.13 \cdot 10^{-7}$ mm for iron [12] and a dynamic viscosity of $1.25 \cdot 10^{-3}$ Pa·s for Pb-17Li at 500°C, one obtains for the diffusivity of iron in Pb-17Li the following value [12]:

$$D_{Fe}(550°C) = 6.4 \cdot 10^{-9} \cdot m^2/s \tag{30}$$

This theoretical value was compared to values of the diffusivity obtained from experiments with a rotating cylinder, which are smaller by a factor of about 10^{-5} [12].

But one should be cautious in applying equation (29) for solutes in liquid metals. As they exist in form of solvated metal clusters. Thus, one should use an effective cluster radius in eq. (29), which can be much larger than the “real” atomic radius. But it seems doubtful whether a factor of 10^{-5} can be explained in this way. The same problem was also discussed in [21]. There an iron solubility, which is lower by a factor of 1000, was favored. This would allow the use of a value of the iron diffusivity much nearer to that given by the Sutherland-Einstein equation.

The authors in ref. [22] have deduced the following correlation for the iron diffusivity from the dissolution rates in crucibles by applying a simple model:

$$D_{Fe}(T) = e^{-19.64 - 2844/T} \text{ in } m^2/s \tag{31}$$

A value of about $1 \cdot 10^{-10}$ m^2/s at 500°C is obtained from this correlation. Fig. 26 shows a comparison of iron diffusion coefficients, calculated by eq. (29) and (31).

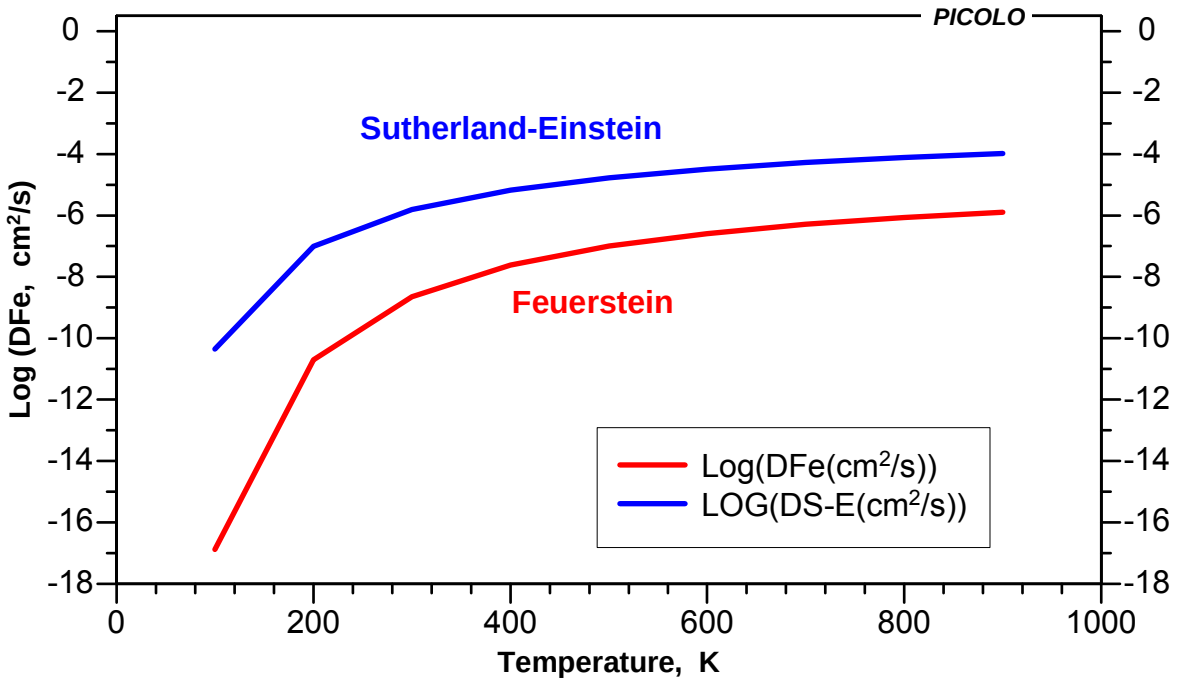

Fig. 26: Iron diffusion coefficient in Pb-17Li versus temperature according to Feuerstein et al. [22] and according to the Sutherland-Einstein correlation

Experimental values of diffusion coefficients in various liquid metals have been collected in ref. [25]. They range in the order of 10^{-5} – 10^{-4} cm^2/s. For iron in liquid lead a value lower than $8.3 \cdot 10^{-6}$ cm^2/s is given for a temperature of 643 K. No values of the diffusion coefficients in Pb-17Li have been provided in [23] except for H and T. The experimental diffusion coefficients are frequently charged with a convectional overestimation, an underestimation is much less probable [25].

For the kinematic viscosity of Pb-17Li the following correlation was given in [19]:

$$\nu_{fl}(T) = 1.9 \cdot 10^{-8} \cdot \exp(1406/T) \text{ in } m^2/s \qquad (32)$$

T = temperature in Kelvin

The viscosity decreases slightly with increasing temperature. Increasing the temperature from 480 to 550°C, would reduce the viscosity of Pb-17Li by about 15%.
The dissolution rates in a loop are mainly determined by the product of the solubility and the mass transfer coefficient and one can estimate the dependence of the dissolution rates on the flow velocity in the loop and on the maximum temperature. If the maximum temperature in the PICOLO loop is increased from 480 to 550°C the iron solubility would increase by a factor of about 11, if the correlation of Borgstedt et al. is correct and increase by a factor of about 1.2, if the correlation of Coen et al. is correct.
In the turbulent flow regime the dissolution rates increase with a power of about 0.9 of the flow velocity, whereas in the laminar regime they would be independent of the flow velocity. In general, diffusion is a slow process compared to chemical reactions. Therefore we assume that the rate constant of the interface reactions, is much higher than the mass transfer coefficient in the liquid metal. Thus, we have:

$$c_{Fe}^{w} = c_{Fe}^{s} \qquad K_t = K_{Fe}^{fl} \tag{33}$$

with c^{W}_{Fe} the iron concentration at the wall and c^{S}_{Fe} the iron solubility in the liquid metal.

This view is generally accepted in the literature (see for example refs. [5, 12]). In case of metallic surfaces, as in the PICOLO loop, we also assume that there is no diffusion layer at the surface of the wall. This condition can be removed, if in the future we can get experimental evidence for such surface layers. According to ref. [18] porous ferritic layer are observed on the surface of austenitic steels which are characterized by a depletion of nickel, manganese and chromium. Ferritic steels, on the other hand show no such surface layer [18]. The presence of porous surface layers could eventually be not observed by metallography, as they may be very friable. They would in any case necessitate the use of an iron diffusivity coefficient in the liquid metal distinctly lower than in reality, if they are not included in the model.

6 Treatment of multi-modular loops

In general, loops will consist of a certain number of sections, which can have different values for the hydraulic diameter and have different geometries (full or annular cross section for example). In order to deal with such situations, we make use of the fact that the fluid mass flow rate is constant along the loop. For the time being we do not foresee a bypass in some part of the loop. The constancy of the mass flow rate is expressed as follows:

$$A_i^{ch} \cdot \rho_i^{fl} \cdot u_i^{fl} = const. \tag{34}$$

i= number of the axial section

In equation (34) we have neglected the contribution of dissolved cladding components, as they comprise only a few wppm. To a first approximation we can also neglect the temperature dependence of the fluid density. The equation of continuity leads then to the following expression for the flow velocity in the different axial sections:

$$u_i^{fl} = u_{ref.}^{fl} \cdot \frac{A_{ref.}^{ch}}{A_i^{ch}} \tag{35}$$

There we have made use of the fact that the nominal flow velocity in the loop is given for some reference axial section.

The hydraulic diameter in a certain axial section is to be calculated with the help of the following formula, applicable also in case of non-circular cross sections:

$$d_{hyd,i} = \frac{4 \cdot A_i^{ch}}{P_i^{ch}} \tag{36}$$

P_i^{ch} = wetted channel perimeter in the axial section i

7 Numerical procedures

Finite difference techniques are applied for the solution of the differential equations and for the calculation of the integrals. In order to do this we have to divide the total loop into a certain number of equal-sized axial meshes. If N_{ax} is the number of the axial meshes, then the axial length Δx of a mesh is given as:

$$\Delta x = L/N_{ax} \tag{37}$$

The axial positions x_i of the boundaries of the i th axial mesh are then:

$$\begin{aligned} x_u &= (i-1)\cdot \Delta x \\ x_d &= i \cdot \Delta x \end{aligned} \tag{38}$$

x_u = upstream end of the i th axial mesh
x_d = downstream end of the i th axial mesh

Then the differential quotient of a function f(x) in the axial mesh is approximated by:

$$\frac{\partial}{\partial x} f(x) \approx \frac{\Delta f}{\Delta x} = \frac{f_d - f_u}{\Delta x} \tag{39}$$

f_d = value of the function f at the downstream end of the axial mesh
f_u = value of the function f at the upstream end of the axial mesh

The contribution of an axial mesh to an integral of the function *f(x)* can be approximated with the help of the trapezoidal rule:

$$\int_{a.m.} f(x)dx \approx 1/2 \cdot (f_u + f_d) \cdot \Delta x \tag{40}$$

8 Iterative procedure

In a closed loop we have the periodic boundary condition (7) for the bulk concentration of a solute i, but we have in general no a priori definite knowledge of the value at the origin of the loop x = 0. If there is a magnetic trap, which removes the solute quantitatively, we could take the axial position of the magnetic trap as the origin of the loop and we would then have the following condition:

$$c_i^b(x=0) = c_{Fe}^{s,m.tr.} \tag{41}$$

The idea behind eq. (41) is that the iron concentration in the liquid metal in the magnetic trap can not fall below the thermodynamic equilibrium value in it. The magnetic trap acts primarily on iron particles and less on iron atoms. For the time being the precipitation of iron particles in the liquid metal is not included in the code. But with the eq. (41) we can describe the maximum effect that a magnetic trap can have.

The calculation of the bulk concentration and of the mass flux from the wall into the liquid metal along the whole loop would then be straightforward and the amount of solute removed in a time interval Δt by the magnetic trap would be determined by:

$$\Delta m_i^{rem.} = u^{fl} \cdot \Delta t \cdot A^{ch} \cdot (c_i^b(x = L) - c_i^b(x = 0)) \tag{42}$$

In the other case one must proceed iteratively. The iterative procedure used in MATLIM is based on the following equation:

$$\int_0^L j_i(x) \cdot U_{ch} \cdot dx = 0 \tag{43}$$

which is an integral formulation of the mass conservation law; no solute disappears from the closed loop.

The following quantity can be calculated from the very beginning, as it depends only on the boundary conditions:

$$jc_i^w = \int_0^L K_i^{fl}(x) \cdot c_i^w(x) \cdot U_{ch} dx \tag{44}$$

The iteration starts then with an initial value for c_i^b at x = 0. Then in a first round of iteration all the other values of c_i^b along the whole loop can be calculated with the help of eqs. (12) and (16). We can then calculate the following quantity:

$$jc_i^b = \int_0^L K_i^{fl}(x) \cdot c_i^b(x) \cdot U_{ch} dx \tag{45}$$

Then we compare jc_i^w to jc_i^b by calculating the following quantity:

$$\text{dev} = ABS((jc_i^b - jc_i^w)/jc_i^w) \tag{46}$$

If the quantity dev is below a certain pre-defined threshold the iteration is finished, otherwise the value of $c_i^b(x=0)$ has to be changed and a new round of iteration starts. The number of iterative cycles N^{iter} is counted in the code. If no convergence is reached after a certain pre-defined number of iterative cycles N^{ult} the calculation is stopped and the whole iterative procedure must be changed somewhat.

9 Structure of the code

The global structure of the MATLIM code can be inferred from the following flow sheet:

Material data

Test data of the loop

Axial meshes

Temperature distribution along the loop, iron concentration at the wall

Selection of the mass flux model

Start of the iterative procedure for the mass transfer coefficient model

$N^{iter} = 1$

Iron flux, iron bulk concentration, oxygen bulk concentration

Convergence criteria fulfilled?

$N^{iter} = N^{iter} + 1$

$N^{iter} \geq N^{ult}$?

Transfer of the relevant results to output data set

Stop

10 Results of calculations for the PICOLO loop with the MATLIM code

A description of the PICOLO loop can be found in ref. [26]. The loop has recently been upgraded to a maximum temperature of about 550°C [27] and the main aim of the calculations with the MATLIM code was to estimate the effect of the temperature increase on the dissolution rates of Fe-Cr steels like EUROFER 97. The dissolution rates are mainly determined by the iron solubility and diffusivity. Hence, the choice of the relevant correlations is essential. The correlations of ref. [22] seem most promising and have therefore been selected for this work.

The PICOLO loop contains different components like an electrical heater, a heat exchanger, a magnetic trap and a test section with test specimens all with different hydraulic diameters and is therefore a multi-modular loop. The treatment of multi-modular loops in the MATLIM code was described in chapter 6. It should be noted that as concerns the magnetic trap only the hydraulic behavior is simulated and not the magnetic trapping effects, as we have for the time being no knowledge on the magnetic field strength in the trap and no knowledge on the size and distribution of iron particles in the liquid metal. The clarification of this issue has to be treated in future investigations.

Fig. 27 shows the axial profiles of the hydraulic diameter and of the flow velocity along the whole loop. The flow velocity has its highest value along the test section loaded with the test specimens and is lowest inside the magnetic trap (1 cm/s). The flow velocity in the test section was calculated to be about 0.22 m/s.

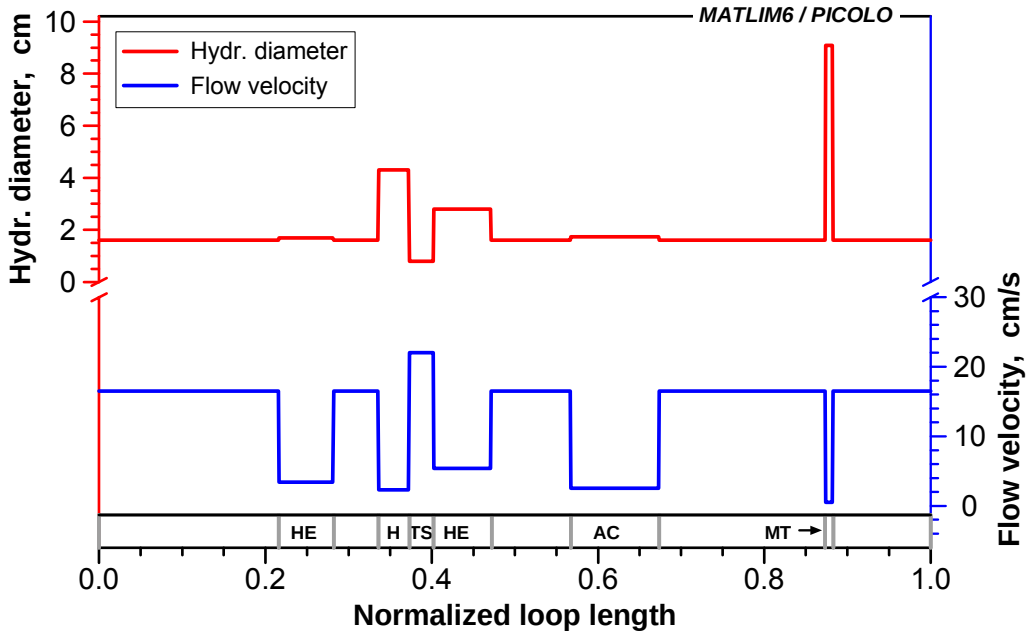

Fig. 27: Axial distributions of the flow velocity and hydraulic diameter in the PICOLO loop

Some of the results of the code calculations, which seem to be of greatest interest to the reader, are to be seen in Figs. 28 - 32 for the low temperature case (maximum loop temperature about 480°C) and the corresponding results for the high temperature case (maximum temperature in the loop about 550°C) in Figs. 33 - 37.

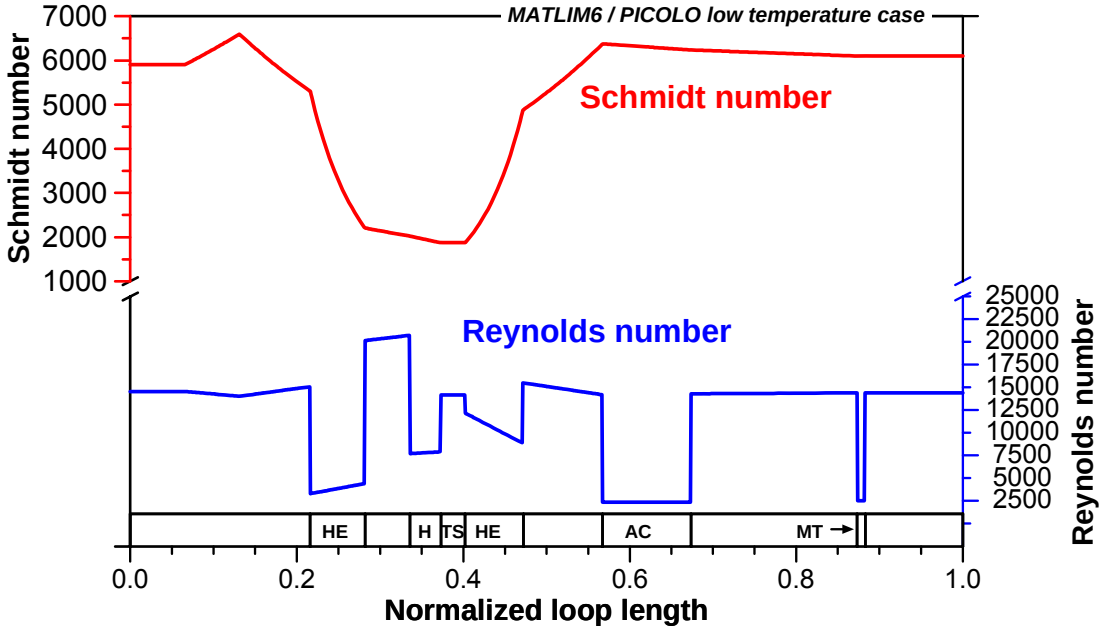

Fig. 28: Axial distributions of the Reynolds and Schmidt number (low temperature case)

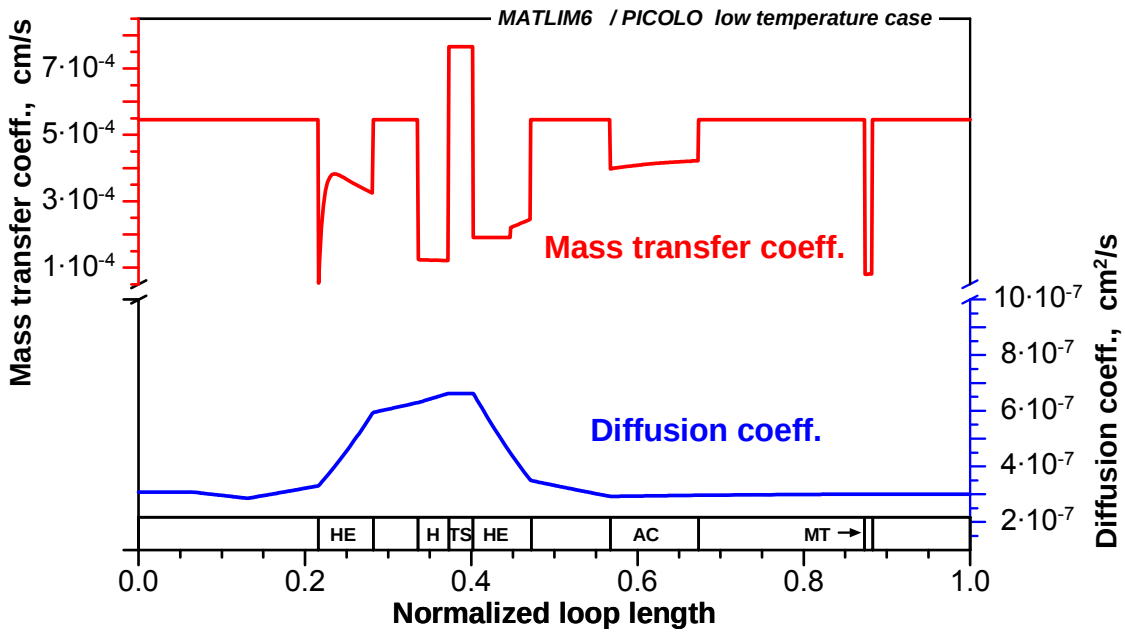

Fig. 29: Axial distributions of the mass transfer and diffusion coefficient in the loop (low temperature case)

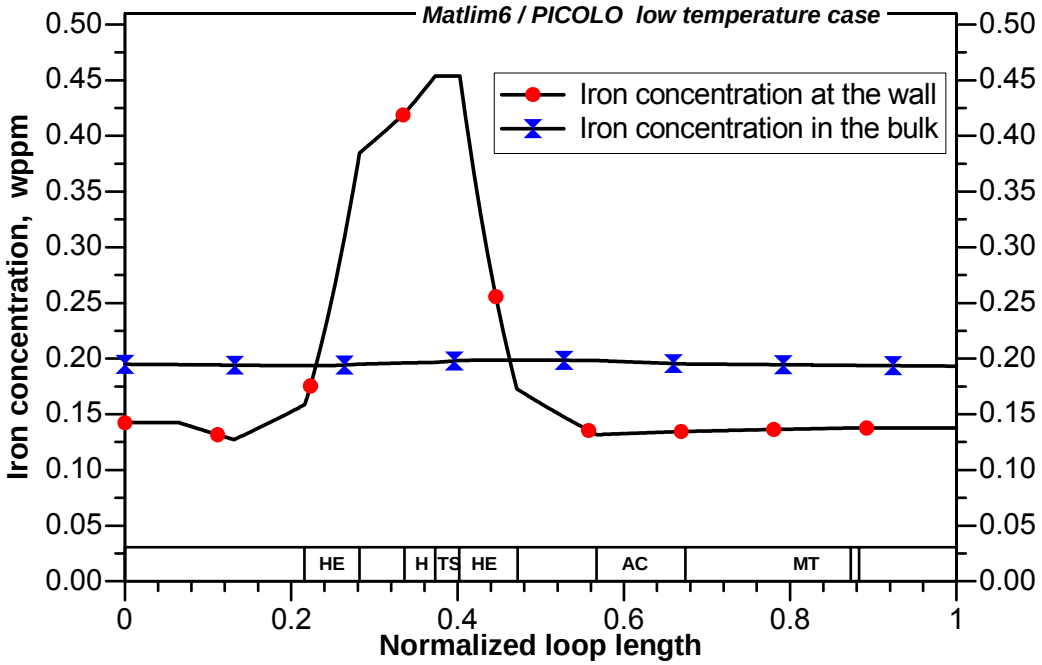

Fig. 30: Axial distributions of the iron concentration at the channel wall (CFEW) and in the bulk of the fluid (CFEB) (low temperature case)

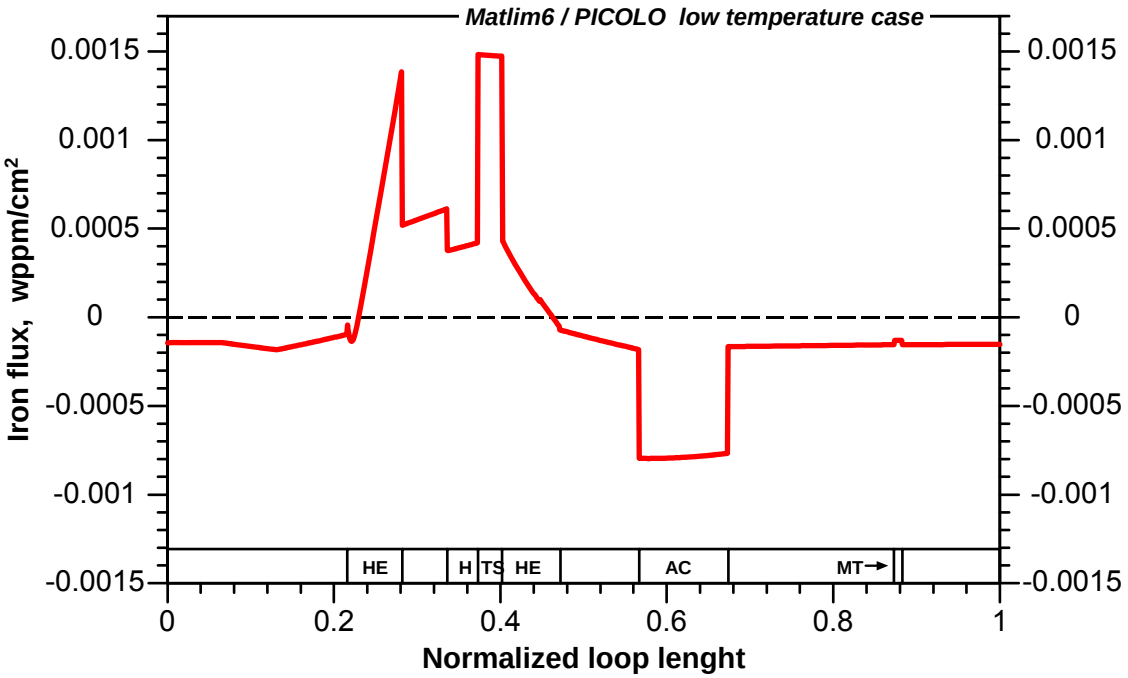

Fig. 31: Axial distributions of the iron flux from the channel wall into the liquid metal (low temperature case)

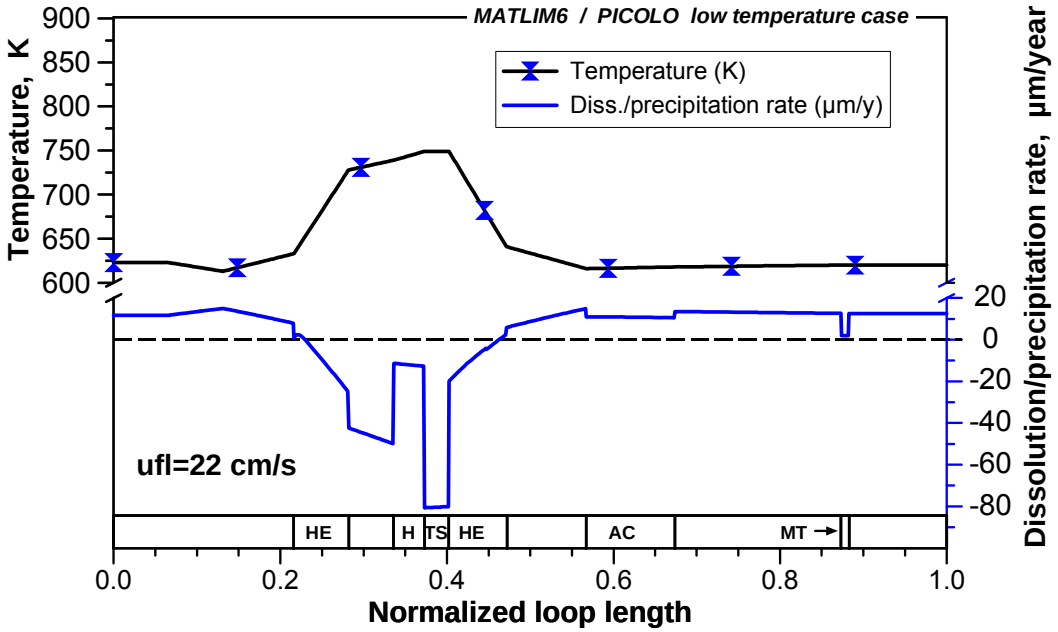

Fig. 32: Axial distributions of the temperature in the loop and of the dissolution/ precipitation rates (low temperature case)

Most interesting are of course the dissolution/precipitation rates along the loop shown in Fig. 32 and 37 for the two cases. It should be noted that due to the convention used in the MATLIM code negative values stand for dissolution and positive values for precipitation. The maximum dissolution rates are to be found in the loaded test section, namely about 80 µm/a in the low temperature case and about 520 µm/a in

the high temperature case. It should be noted that for tests in the PICOLO loop under low temperature conditions for the dissolution rate in the test section values of about 90 µm/a have been reported [28]. For the high temperature case a most reliable value of about 500 µm/a was evaluated as discussed in the testing part of this report with exposure time up to 5000 h.

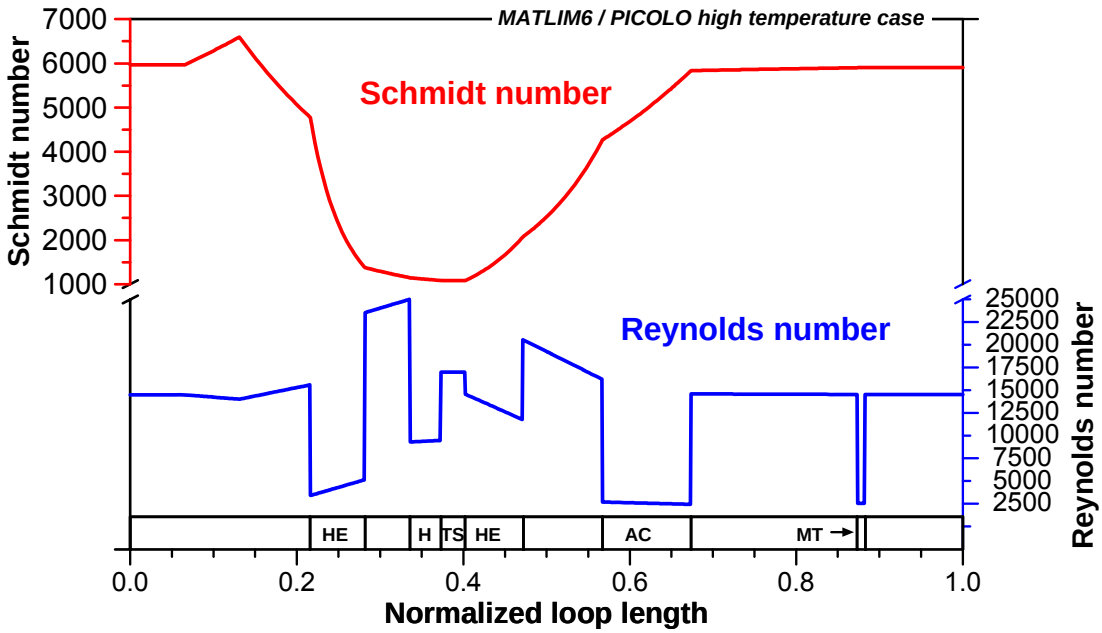

Fig. 33: Axial distributions of the Reynolds and Schmidt number (high temperature case)

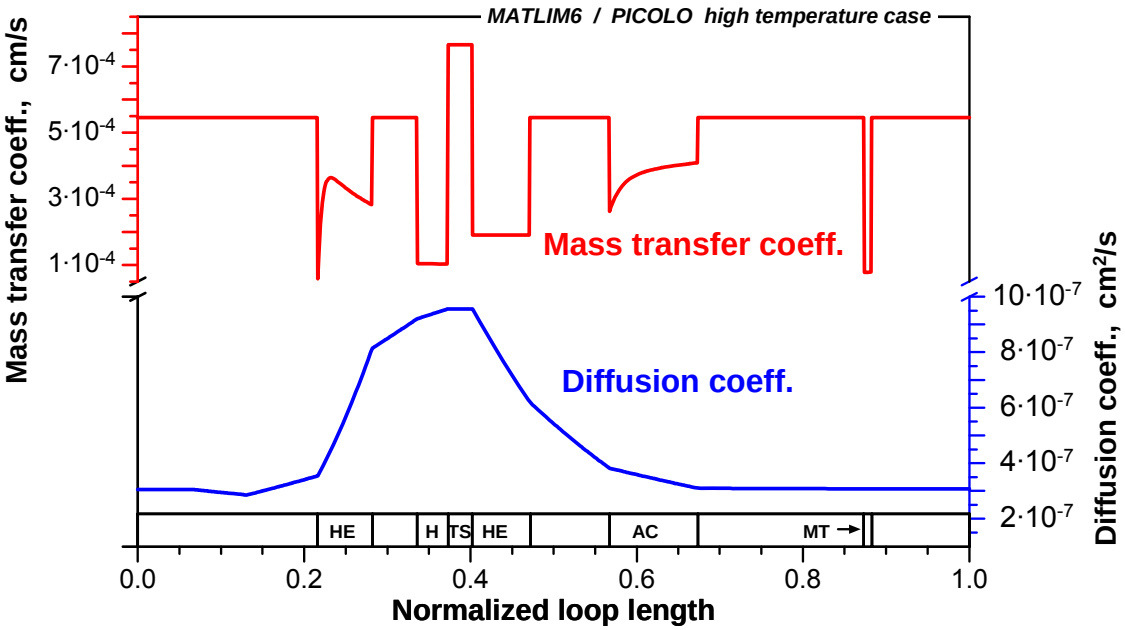

Fig. 34: Axial distributions of the mass transfer and diffusion coefficient in the loop (high temperature case)

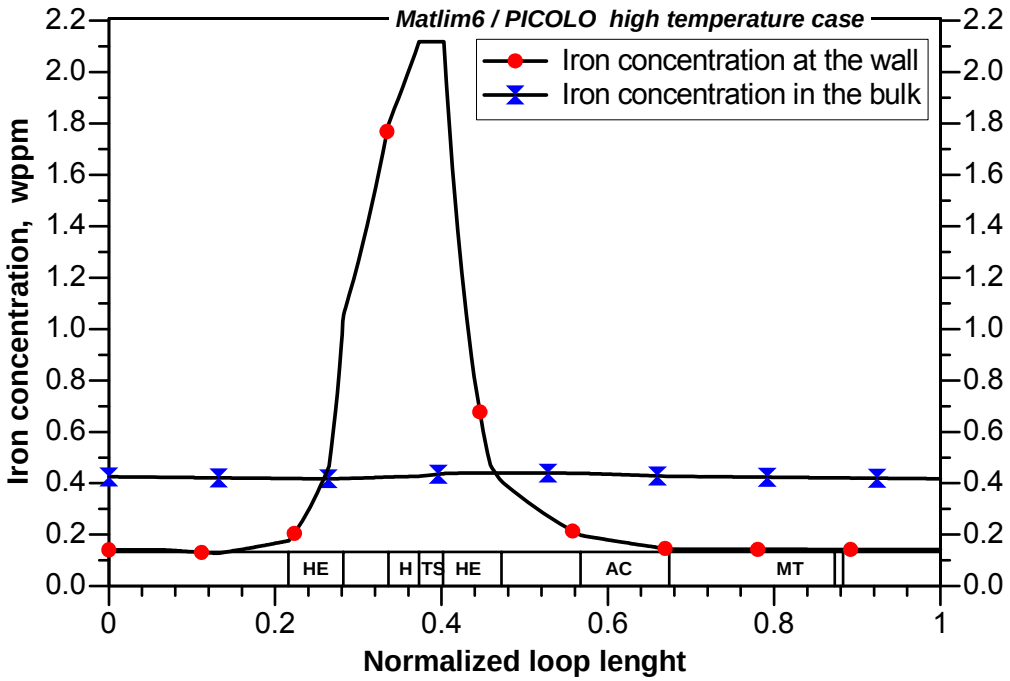

Fig. 35: Axial distributions of the iron concentration at the channel wall (CFEW) and in the bulk of the fluid (CFEB) (high temperature case)

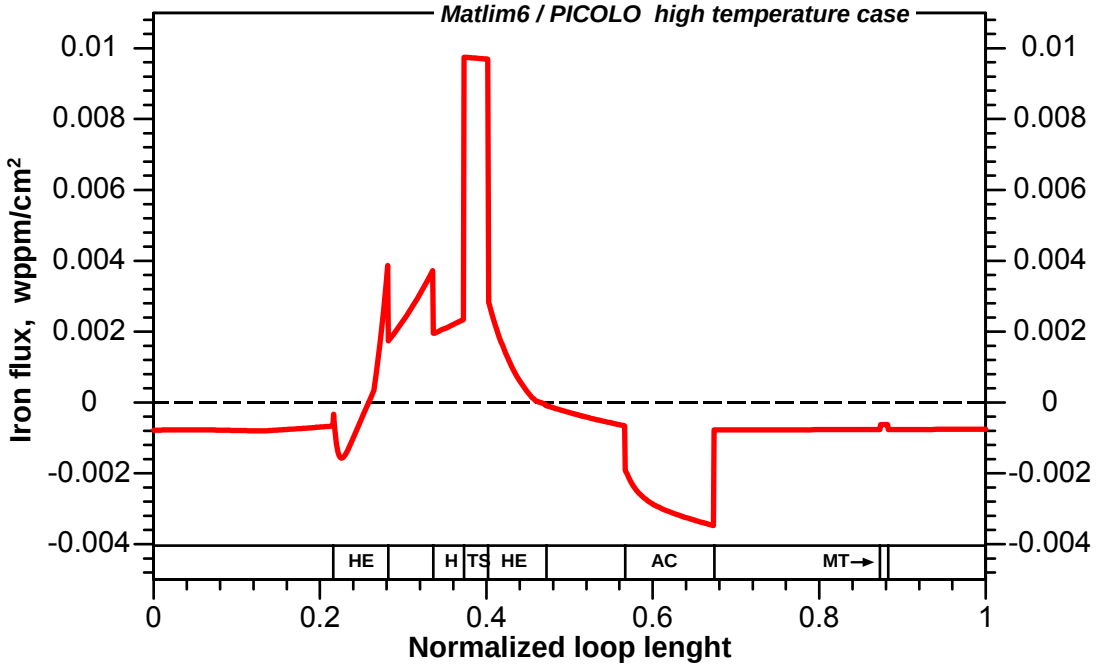

Fig. 36: Axial distributions of the iron flux from the channel wall into the liquid metal (high temperature case)

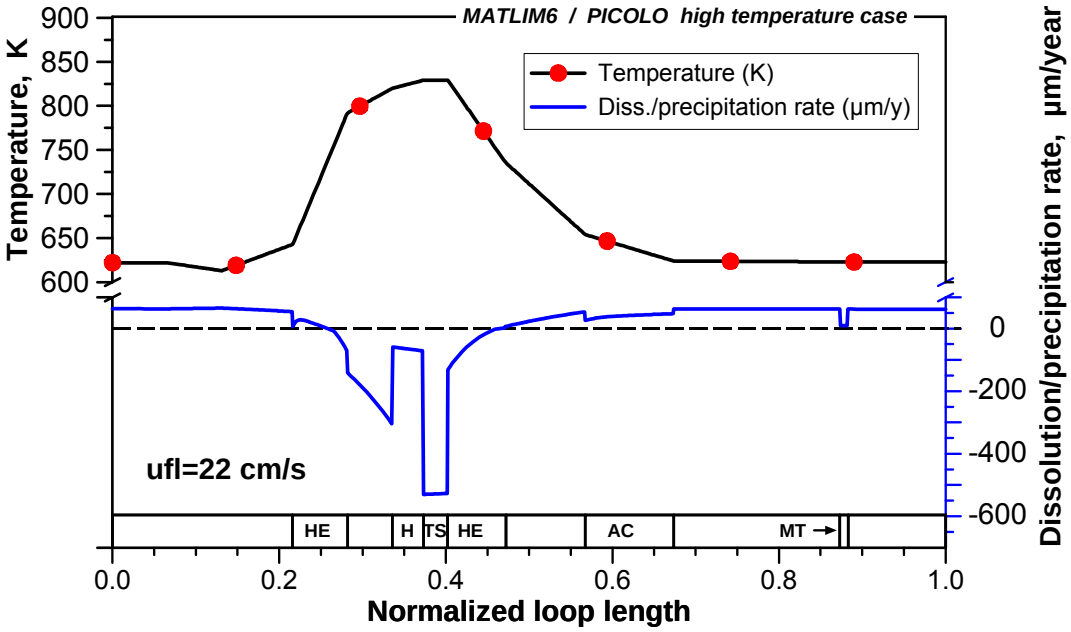

Fig. 37: Axial distributions of the temperature in the loop and of the dissolution/ precipitation rates (high temperature case)

The axial profiles of the dissolution/precipitation rates (Fig. 32 and Fig. 37) are looking rather perturbed as a consequence of the hydraulic properties of the different components. The results plotted in Fig. 27 (velocity and hydraulic diameter) Fig. 28 (Reynolds and Schmidt numbers) and Fig. 29 (diffusion and mass transfer coefficients) should help to understand these profiles, as the dissolution/precipitation rates are determined by the mass transfer coefficient and the difference between the iron concentration at the wall and in the bulk of the fluid. The same is valid for the high temperature case with the Figs 33 (Reynolds and Schmidt numbers) and 34 (diffusion and mass transfer coefficients), respectively. The mass transfer coefficient is mainly determined by the Reynolds and the Schmidt numbers.

The flow is fully turbulent in the test section and in the tubing of the loop but in some components like the magnetic trap, the cooler and electrical heater the Reynolds number is below 10^4 and the flow is therefore in a transition regime. Due to the low values of the iron diffusivity the values of the Schmidt number are rather high, they range between about 2,000 and 6,000. The mass transfer coefficient varies between 10^{-3} and 10^{-2} cm/s. Figs. 30 and 35 show the iron concentration at the wall (CFEW) and the iron concentration in the bulk (CFEB). Fig. 31 and Fig. 36 depict the iron flux from the channel wall into the liquid metal. Negative values of the iron flux mean that the flux is directed from the liquid metal to the wall, leading to precipitation at the wall.

11 Remarks

A kinetic model for the calculation of mass transfer in liquid metal systems under forced convection flow conditions has been developed. It is based on the use of the relevant characteristic thermo-hydraulic numbers, which determine the mass flux from the wall into the fluid. This is supplemented by the application of the mass conservation law to calculate the conditions in the bulk of the fluid. The dissolution/precipitation rates determine then the geometrical changes of the structural components. For metallic surfaces the dissolution rates can be considerable. In this case a lot of experimental data are available. If oxide scales are present the dissolution rates should be very much smaller. Besides the thermo-hydraulic parameters like flow velocity and hydraulic diameter, iron diffusivity and solubility are of the greatest importance. In a first round of calculations for the PICOLO loop we have started to validate the newly developed code MATLIM. For this we have used correlations for the iron solubility and iron diffusivity provided by Feuerstein et al.. These correlations yield reasonable results for the dissolution rates. With the code MATLIM a simple and flexible tool for the calculation of mass transfer and geometrical changes in liquid metal loops is now available at FZK.

In the MATLIM code it is assumed at the moment that precipitation occurs at the channel walls. But there are indications from the PICOLO loop that iron particles can precipitate in the liquid metal. Well, the implementation of metallic and/or oxide particle behavior will be the main aim of the next step of code development. An additional topic may be erosion processes.

Conclusions

The technological work of upgrading PICOLO-loop for corrosion testing of EUROFER at 550°C was conducted as planned and the test campaign up to 5000 h exposure time was successfully finished at a flow velocity of v = 0.22 m/s. The corrosion mechanisms are the same at 550°C as earlier evaluated at 480°C test series, however the corrosion rate is dramatically increased to about 500 µm/a compared to 90 µm/a at 480°C. This large attack yields a dissolved Fe amount of about 4 kg/m² surface area of EUROFER. Considering this huge amount and the fact that precipitates are formed at cooler loop sections due to over-saturation of the Pb-17Li melt the observed loop blockages are reasonable after short operation time of only 3,000 h. The analyses of the precipitation effects showed that only a small part of the corrosion products is deposited at the walls if at all. The huge amount of particles found in the magnetic trap may indicate that precipitates are formed in the Pb-17Li bulk. The newly started work on precipitation and transportation effects can not specify the locations there the particles are formed at this early stage. However, the performed test series clearly showed the risks coming from precipitations regarding loop blockages.

A kinetic model for the calculation of mass transfer in liquid metal systems (Pb-17Li e.g. PICOLO loop) under forced convection flow conditions was set up. It is based on the use of the relevant characteristic physicochemical data and thermo-hydraulic numbers, which determine the mass flux from the wall into the fluid assuming oxygen free surface and underlying a mechanism of dissolving components (Fe) out of the steel. In the frame of this modeling work a literature review concerning Pb-Li corrosion tests was also performed. The main view points were liquid metal flow characteristics and observed / calculated diffusivity data. A critical analysis of these data inclusively discussion of their impact on predicted / calculated results was done and is included in the part modeling. The validation part showed that the tools set up can in general describe the dissolution of the steel components; however the results will be strongly affected by a correct selection of physicochemical data. The predicted corrosion rates for 480°C and 550°C are about 80 µm/a and 520 µm/a; respectively. Both calculated values are in good agreement with the measured data. The modeling tools predict also the precipitation effects in a loop with hot and cold legs, however, additional tools will be required to model the observed bulk effects.

By combination of experimental and modeling work a significant progress was realized especially in the change over from only mechanism-based tests to considering the whole loop behavior under corrosion, transport and precipitation view. Looking on the transport and precipitation effects occurring in a real arrangement first hints are now available due to the results obtained from the modeling work and analyzing first samples cut out of the loop for testing. However, this field requires more additional data for valuation of future measures and estimating the impact on loop operation. Two steps are at least necessary on the short term scale. The first will be the validation of the modeling tools by corrosion rates measured at lower flow rates e.g. at 550°C and, secondly, metallurgical data are urgently required which are describing precipitations at different loop positions for validation of the included dissolution / precipitation tools in modeling.

The performed tests and the results in modeling show clearly that corrosion is a serious problem at high temperatures and will need special measures e.g. corrosion protection by surface coating to reduce the corrosion attack to acceptable limits which guarantee a safe and economic application in TBM's.

Acknowledgement

These corrosion tests were carried out in the framework of the Nuclear Fusion Project of the Forschungszentrum Karlsruhe and supported by the European Fusion Technology program.

The authors wish to thank the following colleagues for their help and assistance:
Dr. C. Adelhelm for the chemical analyses and Mrs. H. Zimmermann and P. Graf for the metallographic investigations.

References

[1] R. Lindau, A. Möslang, M. Schirra, Thermal and mechanical behaviour of the reduced-activation-ferritic-martensitic steel EUROFER, Fusion Eng. Design, 61-62, 2002, 659

[2] W. Krauss, J. Konys, Z. Voss, J. Novotny, Corrosion behaviour of EUROFER 97 in flowing Pb-17Li, Corrosion testing in Picolo loop (480°C), TW1-TTMS-003

[3] J. Konys, W. Krauss, Z. Voss, O. Wedemeyer, Corrosion behaviour of EUROFER steel in flowing eutectic Pb-17Li alloy, J. Nucl. Mat., 329-33 (2004) 1379-1383

[4] J. Sannier, T. Flament, A. Terlain, Corrosion of martensitic steels in flowing Pb17Li, Proc. 16th Symp. Fusion Technology, 3-7 Sept., 1990, London, UK, 901-905.

[5] X. He, N. Li, M. Mineev, J. Nucl. Mat. 297 (2001) 214-219

[6] J. Zhang, N. Li, J. Nucl. Mat. 321 (2003) 184-191

[7] J. Zhang, N. Li, Corrosion 60 (2004) 331-341

[8] J. Zhang, N. Li, J. Nucl. Mat. 326 (2004) 201-210

[9] E. Buckingham, Phys. Rev. 4 (1914) 345- 376

[10] S. Z. Beer, Liquid Metals, Marcel Dekker, Inc., N.Y. (1972) 38-40

[11] C. S. Tedmon, J. Electroch. Soc. 113 (1966) 766 – 768

[12] F. Balbaud-Celerier, F. Barbier, J. Nucl. Mat. 289 (2001) 227-242

[13] F. P. Berger, K. Hau, Int. J. Heat Mass Transfer 20 (1977) 1185

[14] D. C. Silverman, Corrosion 55 (1999) 1115

[15] P. Harriott, R.M. Hamilton, Chem. Eng. Sci. 20 (1965) 1073

[16] Verein Deutscher Ingenieure, VDI-Wärmeatlas Berechnungsblätter für den Wärmeübergang, 8. Auflage 1997, Springer, Berlin Heidelberg, Ga1-Gb5

[17] M. G. Barker, V. Coen, H. Kolbe, J.A. Lees, L. Orecchia and T. Sample, J. Nucl. Mat. 155-157(1988) 732-735

[18] M. G. Barker, T. Sample, Fus. Eng. Des. 14 (1991) 219

[19] H.U. Borgstedt, H. D. Röhrig, J. Nucl. Mat. 179-181 (1991) 596

[20] H.U. Borgstedt, H. Feuerstein, J. Nucl. Mat. 191-194 (1992) 988-991

[21] H.U. Borgstedt, C. Guminski, J. Nucl. Mat. 303 (2002) 240-241

[22] H. Feuerstein, H. Gräbner, J. Oschinski, J. Beyer, S. Horn, L. Hörner, K. Santo, FZKA 5596, Forschungszentrum Karlsruhe (1995)

[23] P. Hubberstey, J. Nucl. Mater. 247 (1997) 208 – 214

[24] M.G. Barker, J.A. Lees, T. Sample, Proc. 4th Int. Conf. Liquid Met. Eng. and Technol., Avignon, Vol. 1 Paper 206 (1984)

[25] C. Guminski in H.U. Borgstedt, Liquid Metal Systems Material Behavior and Phys. Chem. in Liquid Metal Systems 2, 345, Plenum Press, N.Y. (1995)

[26] H. Glasbrenner, J. Konys, Z. Voss, J. Nucl. Mat. 281 (2000) 225-230

[27] W. Krauss, J. Konys, H. Steiner, J. Novotny, Z. Voss. O. Wedemeyer, EFDA report

[28] J. Konys, W. Krauss, Z. Voss, O. Wedemeyer, J. Nucl. Mat. 303 (2002) 240-241